GEODYNAMICS & TECTONOPHYSICS
Published by the Institute of the Earth's Crust, Siberian Branch, Russian Academy of Sciences

PALEOGEODYNAMICS

2022 VOLUME 13 ISSUE 1 ARTICLE 0573

ISSN 2078-502X

DOI: 10.5800/GT-2022-13-1-0573

GEOLOGICAL SETTING AND GENESIS OF THE KURMANSKY GABBRO-TRONDHJEMITE MASSIF (MIDDLE URALS)

S.V. Pribavkin ✉, A.V. Korovko, M.D. Vishniakova

Zavaritsky Institute of Geology and Geochemistry, Ural Branch of the Russian Academy of Sciences, 15 Academician Vonsovsky St, Ekaterinburg 620016, Russia

ABSTRACT. This paper reports the results of petrogeochemical studies of the Kurmansky gabbro-trondhjemite massif (eastern slope of the Middle Urals), lying in the western part of the large Reftinsky allochthonous block within the accretion East Uralian megazone. The relevance of this study is determined by the uncertainty in geodynamic setting and formation conditions of the rock massif and its role in the evolution of the Ural Mobile belt. We specified the countours of the massif. It is shown that the rocks were resulted from spatiotemporal convergence of partial melting in the mantle and lower crust at the island-arc stage of the Ural Mobile belt evolution. Partial melting of mantle peridotite, under the influence of an aqueous fluid rising from the subduction zone, initiated the occurrence of basite melts. The separation of the melt and its subsequent evolution to the compositions of gabbrodiorite and diorite took place at P_{tot}=10 kbar. Trondhjemites were formed as a result of partial melting of amphibolites at P_{tot}≥8 kbar, P_{H_2O}=0.1–0.2 kbars. The crystallization of trondhjemites in the crust was accompanied by the wollastonite skarns on contact with carbonate rock and xenoliths culminated at mesoabyssal level, P_{tot}=P_{H_2O}=1 kbar. The comparison between the composition of Kurmansky gabbro-trondhjemite massif and the island-arc- and collision-related magmatic suites in the region allowed us to assume that the Kurmansky massif belongs to the independent Early Devonian (?) gabbro-trondhjemite complex of island arc origin. The rock metamorphism conditions were evaluated, with the transformations supposedly related to the accretion of early island arc complexes at the Murzinsky-Aduysky microcontinent, which took place in the Devonian.

KEYWORDS: petrology; geochemistry, gabbro; trondhjemites; Kurmansky massif; Reftinsky allochthon; Middle Urals

FUNDING: The work is done under the government contract of IGG UB RAS, theme AAAA-A18-118052590029-6, with the equipment of Shared Research Facilities "Geoanalytic" in IGG UB RAS. The modernization and integrated development of Shared Research Facilities "Geoanalytic" in IGG UB RAS is provided with financial support of the grant of the Ministry of Science and Higher Education of the Russian Federation, Agreement 075-15-2021-680.

RESEARCH ARTICLE

Received: December 25, 2020
Revised: July 8, 2021
Accepted: July 12, 2021

Correspondence: Sergey V. Pribavkin, pribavkins@gmail.com

FOR CITATION: Pribavkin S.V., Korovko A.V., Vishniakova M.D., 2022. Geological setting and genesis of the Kurmansky gabbro-trondhjemite massif (Middle Urals). Geodynamics & Tectonophysics 13 (1), 0573. doi:10.5800/GT-2022-13-1-0573

ГЕОЛОГИЧЕСКАЯ ПОЗИЦИЯ И ГЕНЕЗИС КУРМАНСКОГО ГАББРО-ТРОНДЬЕМИТОВОГО МАССИВА (СРЕДНИЙ УРАЛ)

С.В. Прибавкин, А.В. Коровко, М.Д. Вишнякова

Институт геологии и геохимии им. А.Н. Заварицкого УрО РАН, 620016, Екатеринбург, ул. Академика Вонсовского, 15, Россия

АННОТАЦИЯ. В статье представлены результаты петрогеохимических исследований пород Курманского габбро-трондьемитового массива (восточный склон Среднего Урала), залегающего в западной части крупного Рефтинского аллохтонного блока, локализованного в пределах Восточно-Уральской мегазоны аккреционной природы. Актуальность исследований заключается в установлении геодинамических режимов формирования пород, их позиции в эволюции Уральского подвижного пояса. В ходе исследования уточнены контуры массива. Показано, что данные породы образовались в результате сближенных по времени и в пространстве процессов частичного плавления в мантии и нижней коре на островодужном этапе развития Уральского подвижного пояса. Частичное плавление мантийного перидотита под воздействием восходящего из зоны субдукции водного флюида привело к зарождению базитового расплава. Отделение расплава и его последующая эволюция до составов габбро-диорита, диорита происходили при $P_{общ}$=10 кбар. Трондьемиты, ассоциированные с габброидами, были получены в результате частичного плавления амфиболитов при $P_{общ}$≥8 кбар, P_{H_2O}=0.1–0.2 $P_{общ}$. Их становление в коре сопровождалось развитием волластонитовых скарнов на контактах с ксенолитами карбонатных пород и завершилось в мезоабиссальной обстановке при $P_{общ}$=P_{H_2O}=1 кбар. Выполнено сопоставление состава слагающих массив пород с развитыми в районе магматическими образованиями островодужной и коллизионной стадий, что позволило высказать предположение о принадлежности Курманского массива к самостоятельному раннедевонскому (?) габбро-трондьемитовому комплексу островодужной природы. Охарактеризованы условия метаморфизма пород массива, высказано предположение о связи этих преобразований с аккрецией раннеостроводужных комплексов на Мурзинско-Адуйский микроконтинент, имеющей место в девоне.

КЛЮЧЕВЫЕ СЛОВА: петрология; геохимия; габбро; трондьемиты; Курманский массив; Рефтинский аллохтон; Средний Урал

ФИНАНСИРОВАНИЕ: Работа выполнена в рамках государственного задания ИГГ УрО РАН, тема № АААА-А18-118052590029-6 с использованием оборудования ЦКП «Геоаналитик» ИГГ УрО РАН. Дооснащение и комплексное развитие ЦКП «Геоаналитик» ИГГ УрО РАН осуществляется при финансовой поддержке Министерства науки и высшего образования Российской Федерации, Соглашение № 075-15-2021-680.

1. INTRUDUCTION

An interaction between intensively tectonizied Paleozoic formations and highly metamorphosed Precambrian complexes is one of the key issues in understanding the geological history of development of the Ural Mobile belt. The Late Proterozoic metamorphic rocks of the Murzinsko-Aduysky terrain (a fragment of the Pre-Uralian microcontinent) on the eastern slope of the Middle Urals contact with the Early Paleozoic volcanic and sedimentary complexes (Fig. 1). The time of occurrence and the nature of this contact still remain unclear since collision processes in the Late Paleozoic gave rise to the formation of suture zone and a thick zone of folded rock, followed by the development of shariages and allochtones, and to that of collision granite magmatism – Murzinsky, Aduysky and Kamensky interformation massifs which occupied the junction zone. In this context, the studies of the Reftinsky allochtonous block which is gently overlying the folded zone and primarily composed of the Early Paleozoic magmatic complexes, and the time of occurrence and nature of their metamorphism near their junction with the terrain allow identifying ways to solve the problem mentioned.

The Reftinsky allochtonous block is one of the largest in the Urals (Fig. 1). Besides gabbro, diorites, tonalities and plagiogranites of the Reftinsky complex, in its western part contacting with the interformation granite bodies there are also the rocks of the Alapaevsk dunite-harzburgite-gabbro complex and granitoides of the Averinsky complex [State Geological Map..., 2015, 2017]. There also occur gabbro, gabbrodiorites and trondhjemites of the small Kurmansky massif. The latter, due to the lack of reliable petrogeochemical and geochronological data, were to different extents assigned to either formations of the Reftinsky gabbro-diorite-tonalite-plagiogranite complex [State Geological Map..., 1987] or to those of the Averinsky diorite-trondhjemite complex [Rapoport, Medyakov, 1974] of the Silurian-Early Devonian island arc, or presumably include in the area of the collisional Kamensky granodiorite-granite complex linking tectonic plates of the allochtonous block [State Geological Map..., 2017].

Age- and formation-related attribution of the rocks of the Kurmansky massif was largely contributed to by the works of G.B, Fershtater. In 2013–2015, there appeared a number of publications, including the monograph titled

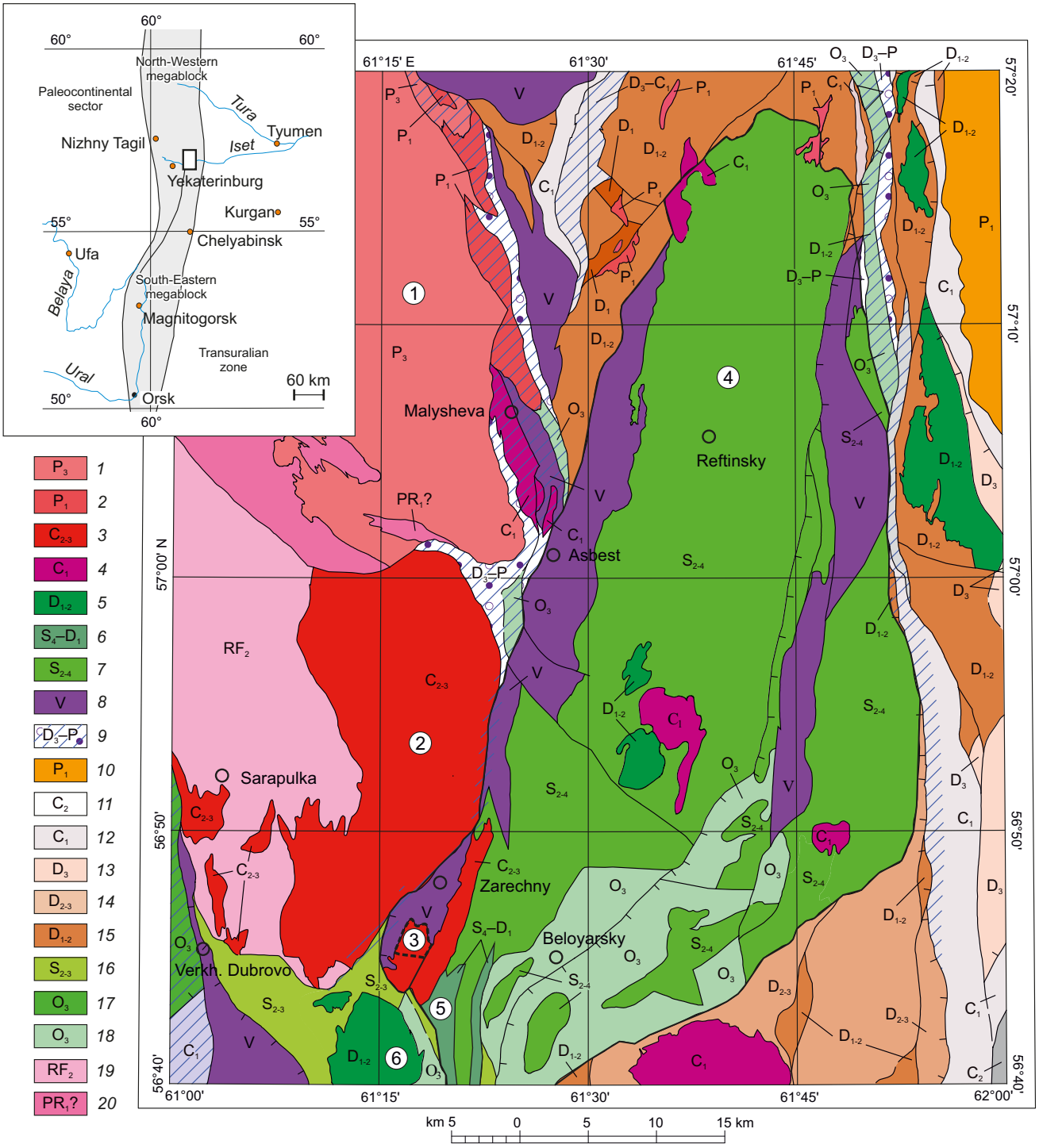

Fig. 1. Geological structure of the Kurmansky massif area (generalized part of the geological map 1: 200000, O-41-XXVI (Asbest) (after [State Geological Map..., 2017]).

Magmatic complexes: *1* – biotite and two-micas granites of the Aduysky complex (P_3); *2* – biotite granites, leucogranites of the Petukhovsky complex (P_1); *3* – granodiorites, granites of the Kamensky complex (C_{2-3}); *4* – gabbro, granodiorites, granites of the Nekrasovsky complex (C_1); *5* – diorites, plagiogranites of the Altay complex (D_{1-2}); *6* – trondhjemites of the Averinsky complex (S_4–D_1); *7* – gabbro, diorites, tonalites, plagiogranites of the Reftinsky complex (S_{2-4}); *8* – gabbro, undifferentiated ultramafites of the Alapaevsky complex (V); *9* – polycomponent melange of the East Uralian tectonogenic complex (D_3–P). Volcanics and volcano-sedimentary and sedimentary complexes: *10* – flasks, sandstones of the Serovsky Suite (P_1); *11* – mudstones, siltstones, sandstones, conglomerates of the Scherbakovsky Suite (C_2); *12* – oligomictic and greywacke sandstones, siltstones, often carbonaceous, siliceous, carbon-siliceous shales of the Aramilsky Suite (S_1); *13* – limestones of the Ustinovsky Suite (D_3); *14* – basalts, andesite-basalts with layers of tuffites, clay-siliceous and siliceous rocks of the Maminsky Formation (D_{2-3}); *15* – subvolcanic rhyolites of the Rudyansky complex (D_{1-2}); *16* – siliceous, carbonaceous-siliceous shales, quartzites, lenses of marbles of the Kolodinsky Suite (S_{2-3}); *17* – metabasalts, metatufosandstones, siliceous tuffites, carbon-quartz rocks of the Novoberezovsky Formation (O_3); *18* – metabasalts, carbon-quartz shales of the Beloyarsky Formation (O_3); *19* – biotite-(Muscovite) – plagioclase-quartz, quartz-amphibole-biotite-plagioclase, (biotite)- amphibole-quartz-plagioclase graphite-containing

shcists, micaceous quartzites, calcifiers, plagiogneisses of the Alabashka suite (RF_2); *20* – of biotite, biotite-amphibole, amphibole-biotite plagiogneisses with layers of amphibolites, granitogneisses (PR_1?).
Figures in circles mean intrusive massifs: 1 – Aduysky, 2 – Kamensky, 3 – Kurmansky, 4 – Reftinsky, 5 – Averinsky, 6 – Brusyansky. A thick solid line shows the contour of the Reftinsky allochthon. Thick dotted line shows the contour of the Kurmansky massif in according to the results of our research.

Рис. 1. Геологическое строение района Курманского массива (генерализованный фрагмент геологической карты образований листа O-41-XXVI (Асбест), масштаб 1:200000 [State Geological Map., 2017]).
Магматические комплексы: *1* – граниты биотитовые и двуслюдяные адуйского комплекса (P_3); *2* – граниты биотитовые, лейкограниты петуховского комплекса (P_1); *3* – гранодиориты, граниты каменского комплекса (C_{2-3}); *4* – габбро, гранодиориты, граниты некрасовского комплекса (C_1); *5* – диориты, плагиограниты алтынайского комплекса (D_{1-2}); *6* – трондьемиты аверинского комплекса (S_4–D_1); *7* – габбро, диориты, тоналиты, плагиограниты рефтинского комплекса (S_{2-4}); *8* – габбро, нерасчлененные ультрамафиты алапаевского комплекса (V); *9* – полимиктовый меланж Восточно-Уральского тектоногенного комплекса (D_3–P). Вулканогенные, вулканогенно-осадочные и осадочные комплексы: *10* – опоки, песчаники серовской свиты (P_1); *11* – аргиллиты, алевролиты, песчаники, конгломераты щербаковской свиты (C_2); *12* – граувакковые и олигомиктовые песчаники, алевролиты, часто углеродистые, сланцы кремнистые, углеродисто-кремнистые арамильской свиты (C_1); *13* – известняки устькодинской свиты (D_3); *14* – базальты, андезибазальты с прослоями туфитов, глинисто-кремнистых пород и кремнистых пород маминской толщи (D_{2-3}); *15* – субвулканические риолиты рудянского комплекса (D_{1-2}); *16* – кремнистые, углеродисто-кремнистые сланцы, кварциты, линзы мраморов колюткинской свиты (S_{2-3}); *17* – метабазальты, метатуфопесчаники, кремнистые туффиты, углеродисто-кварцевые породы новоберезовской толщи (O_3); *18* – метабазальты, углеродисто-кварцевые сланцы белоярской толщи (O_3); *19* – кристаллосланцы биотит-(мусковит)-плагиоклаз-кварцевые, кварц-амфибол-биотит-плагиоклазовые, (биотит)-амфибол-кварц-плагиоклазовые графитсодержащие, кварциты слюдистые, кальцифиры, плагиогнейсы алабашской серии (RF_2); *20* – плагиогнейсы биотитовые, биотит-амфиболовые, амфибол-биотитовые с горизонтами амфиболитов, гранитогнейсов ($PR_{1?}$).
Цифры в кружках – интрузивные массивы: 1 – Адуйский, 2 – Каменский, 3 – Курманский, 4 – Рефтинский, 5 – Аверинский, 6 – Брусянский. Толстой сплошной линией показан контур рефтинского аллохтона. Толстой пунктирной линией показан контур Курманского массива по результатам наших исследований.

"Paleozoic intrusive magmatism of the Middle and South Urals" [Fershtater, 2013, 2015], which contain the absolute age determinations of rocks of the Kurmansky massif from zircons (U-Pb method) yielded 411±2 (SHRIMP-II), 397±2 (LA-ICP-MS) Ma for migmatized amphibole gabbro and 405±4 (SHRIMP-II) Ma for trondhjemites. These datings implied that the Kurmansky massif formations could not appropriately be assigned to either Reftinsky (435–430 Ma) or Averinsky (420–419 Ma) complexes, much less to the 309–298 Ma (Late Carboniferous), as it goes in the legend to the latest geological map [State Geological Map..., 2017].

Besides age determinations, G.B. Fershtater and his coauthors put special emphasis on the structure and composition of the massif rocks. It was shown that the presence of intergranular fine quartz-feldspar aggregate is their most important petrographical feature indicative of migmatization process occurrence. This made it possible to project a hypothesis of spontaneous migmatization of hydrous melts of gabbro during their movement to the surface [Fershtater, 2013, 2015; Fershtater et al., 2018; Zamyatina, Borodina, 2015] onto genesis of the rocks of the Kurmansky massif. The pressure during migmatization were estimated by these authors as 8 kbar.

The paper presents the results of the mineralogical and petrogeochemical studies of the rocks of the Kurmansky massif based on the data produced by the authors and their predecessors. It is the contribution to understanding of genesis and formation relation of the massif rocks and to some aspects of the geological structure and history of region evolution including the time of accretion of the Early Paleozoic island-arc complexes with the rocks of the Murzinsky-Aduysky terrain.

2. GEOLOGICAL POSITION AND STRUCTURE OF THE KURMANSKY MASSIF

The Kurmansky gabbro-trondhjemite massif is 40 km eastward of Ekaterinburg among intensively tectonized structures of the East Uralian megazone representing a compound accretion megablock [Puchkov, 2000]. The massive is in the western marginal part of the Reftinsky allochtonous block among steeply east-dipping tectonic plates thrusted on the Murzinsko-Aduysky metamorphic block (terrain or a fragment of the Precambrian microcontinent) and dissected near their junction with the Bazhenov suture zone [Smirnov et al., 2019] "sealed" by the Late Paleozoic granite massifs (Fig, 1).

According to the results of our earlier complex interpretation and newly obtained data, the Kurmansky massif is almost subisometric, of size 3.5×2 km (Fig. 1), more compact than was supposed [State Geological Map..., 2017]. The massif is composed of gabbro, gabbro-diorites of the first phase and trondhjemites of the second phase, with the predominance of the latter. The rocks in the massif have tectonic contacts with intrusive and volcanic host rocks, and their intrusive contacts with gabbro of the Alapaevsk complex [State Geological Map..., 2017], underlying the allochtonous block, are only marked in the northwest. All rocks in the massif and its nearest environment experienced metamorphism of the epidote-amphibolite facies which gave rise to the formation of amphibolites, metagabbro, and metatrondhjemites. Metamorphic transformations were expressed in the development of amphibole, biotite, epidote, fine-grained granoblastic aggregate of plagioclase and quartz [Eselevich, Sergeevskaya, 1953; Rapoport, Medyakov, 1974]. In spite of the fact of metamorphism, we will further name the rocks in accordance with their primary nature, as it

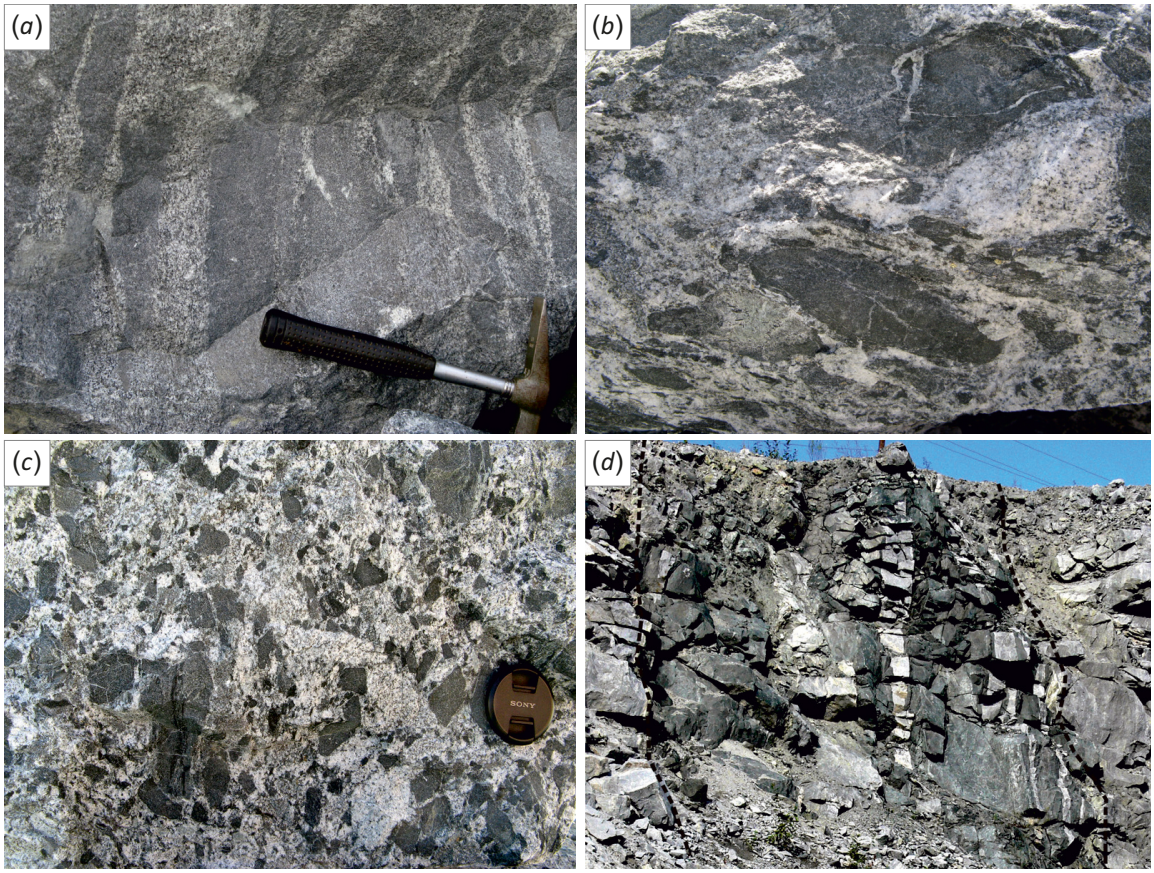

Fig. 2. Relationships of rocks and their geological features.
(*a, b*) – migmatite-like textures in blocks of gabbrodiorites; (*c*) – eruptive breccias of gabbrodiorites; (*d*) – dike of microgabbrodiorites with separations of trondhjemite veins (photo by G.B. Fershtater).

Рис. 2. Взаимоотношения пород и их геологические особенности.
(*a, b*) – мигматитоподобные текстуры в блоках габбро-диоритов; (*c*) – эруптивные брекчии габбро-диоритов; (*d*) – дайка микрогаббро-диоритов с обособлениями жильных трондьемитов (фото Г.Б. Ферштатера).

takes place in explanatory notes to geological maps of the region [Rapoport, Medyakov, 1974; State Geological Map..., 1987, 2017].

A fragment of the northern part of the massif was opened by the Kurmansky broken stone quarry exposing intrusive contacts of trondhjemites with gabbro, gabbro-diorites and diorites. The latter in the contact zone compose large (tens of meters) xenoliths dissected by thin trondhjemite veins (Fig, 2, a, b), described in [Fershtater, 2013, 2015; Fershtater et al., 2018; Zamyatina, Borodina, 2015] as migmatites, or consist of fragments as part of eruptive breccias (Fig. 2, c). Trondhjemites sometimes contain rare xenoliths of metavolcanic and limestone rocks transformed into pyroxene-garnet-wollastonite, garnet-epidote and epidote-quartz-plagioclase skarns [Eselevich, Sergovskaya, 1953; Rapoport, Medyakov, 1974; Pribavkin et al., 2014]. All massif rocks are cut by dykes of microgabbrodiorite and microdiorite with leucocratic segregation veins (Fig. 2, d).

3. PETROGRAPHY OF ROCKS

Macroscopically, gabbro, gabbrodiorites and diorites are unevenly-grained rocks consisting of approximately equal proportions of feldspar and amphibole. Mineral content is as follow (wt. %): plagioclase 30–40, amphibole 35–50, quartz 5–10, epidote and biotite 2–10. The rocks keep the relics of the original gabbro and diorite structure, less often porphyric with predominance of larger-size and idiomorphic amphibole over plagioclase. Relic plagioclase embedded in large subidiomorphic matrices varies in composition from An_{42} to An_{30} and contains epidote inclusions. On the edges and along the fractures, it undergoes recrystallization producing fine- and micro-grained granoblastic aggregate of newly formed plagioclase of composition $An_{20–24}$. The amount of the latter varies from a few percent (Fig. 3, a) to tens of percent, up to complete recrystallization of primary plagioclase (Fig. 3, b). Blue-green amphibole, along with fine long prismatic grains, is embedded in wide matrices (on pyroxene?) with curved splintery contours. Biotite is associated with fine-grained feldspar aggregate indicating its recrystallization-related genesis.

Microgabbrodiorite and microdiorite dykes are characterized by fine-grained nematogranoblastic structure (Fig. 3, c). Orientation of amphibole prisms is irregular or subparallel to dyke contacts. The mineral composition is similar to that of gabbrodiorites described above; the difference lies in the absence of plagioclase above An_{25}.

Trondhjemites are massive, fine-grained rocks containing a large amount of xenoliths. They have the NW-oriented gneissic texture, with numerous xenoliths oriented in the same direction. The massif-predominant trondhjemites contain 30–40 % of plagioclase, 25–35 % of quartz, 5–10 % of biotite, 0–5 % of amphibole, and a small amount of or almost no microcline. Microscopically, they have a primary magmatic middle-grained structure, erased, as well as in gabbroids, by the newly formed micro- and fine-grained granoblastic quartz-feldspar aggregate. The percentage of the latter by volume varies from a few percent, with "a string of beads" formed by single grains (Fig. 3, d), to tens of percent, with only singe primary plagioclase relics kept in the rocks (Fig. 3, e, f). Primary plagioclase corresponds to $An_{24–25}$, and newly formed is similar to it in composition – $An_{20–24}$. Potassium feldspar is only found in newly formed aggregate in much smaller quantities than plagioclase. Biotite is represented by grain seggregations. Blue-green smphibole occurs near the contacts with gabbroids and forms elongated prismatic grains.

Vein trondhjemits are common among gabbroid blocks and dykes making them look like migmatite rocks. They differ from the main trondhjemite phase by larger quantities of amphibole and smaller quantities of quartz. A gradual increase in the amount of dark-colored minerals towards the contact with gabbroids implies trondhjemite contamination with the development of hybrid rocks similar to tonalities or quartz diorites in composition.

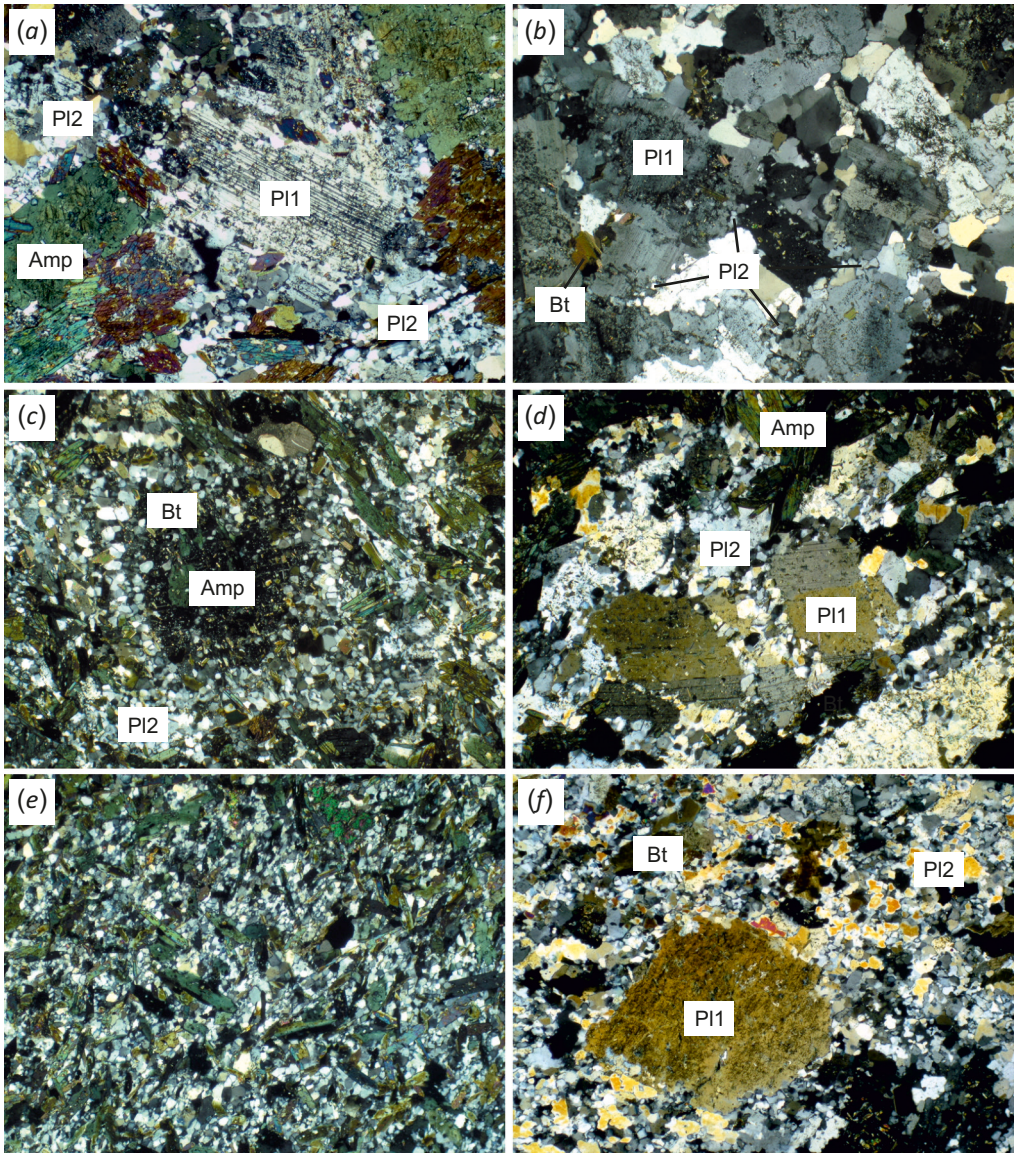

Fig. 3. Micro-images of rock structures: gabbro (*a, b*), microgabbrodiorite (*c*), trondhjemite (*d, e, f*).
The length of the photo is 10 mm. Nicoli crossed. Pl1 and Pl2 are relict and newly formed plagioclas. Amp – amphibole, Bt – biotite. For explanations see the text.

Рис. 3. Микрофотографии структур пород габбро (*a, b*), микрогаббро-диорита (*c*), трондьемита (*d, e, f*).
Длина фотографии – 10 мм. Николи скрещены. Pl1 и Pl2 – реликтовый и новообразованный плагиоклаз. Amp – амфибол, Bt – биотит. Пояснения в тексте.

Accessory minerals in all rock types are represented by apatite, ilmenite-hematite solid solution, magnetite, sulfides, zircons, and titanite. The main secondary mineral is epidote.

The important petrographic feature of the massif rocks, already noted from the results of geological mapping [Eselevich, Sergovskaya, 1953; Rapoport, Medyakov, 1974], is the presence of intergranular fine-grained quartz-feldspar microgranoblastic aggregate interpreted as a result of recrystallization. The relation of this aggregate with migmatization process in which anatectic melt was preserved in situ is particularly emphasized in [Fershtater, 2013; Zamyatin, Borodina, 2015].

4. RESEARCH METHODS

The study of chemical composition of minerals and rocks was performed at "Geoanalitik" Common Use Center IGG UB RAS. The mineral composition was determined by the electron probe micro-analyzer (EPMA) CAMECA SX10 using accelerating voltage 15 kV and current probe 40 nA.

The chemical composition of rocks was determined using X-ray fluorescence spectrometers SRM-35 и XRF 1800. FeO was determined by titration method, ignition losses – by gravimetric method. Trace, rare and rare-earth elements in rocks were determined by the ELAN 9000 ICP-MS System.

The work involved the data on chemical composition of the Kyrmansky rock massif collected over several time periods by the chemical analysis laboratory of the CL PGA "Uralgeologiya" [Rapoport, Medyakov, 1974; Kubashin, Lykova, 1985].

5. RESULTS

5.1. Characteristics of chemical composition of the rocks

On the classification diagram, the total alkali – silica, xenoliths and mafic dykes correspond to gabbro, gabbrodiorites and diorites, and the main trondhjemite phases – to granite and leucogranite (App. 1, Table 1; Fig. 4). Vein trondhjemites intruding gabbroids lie in fields of quartz diorites, granodiorites and granites and represent variously contaminated leucogranite varieties. All rocks are characterized by Na predominance over K, but gabbroids characterized by medium-potassium content, and granitoids – by low-potassium content (Fig. 5). Low-potassium composition allows you to define them as tonalites and trondhjemites.

Trondhjemites of the Kurmansky massif have a relatively low value of FeO/(FeO+MgO) [Frost et al., 2001] equal to 0.65–0.76 and are located in the field of magnesium

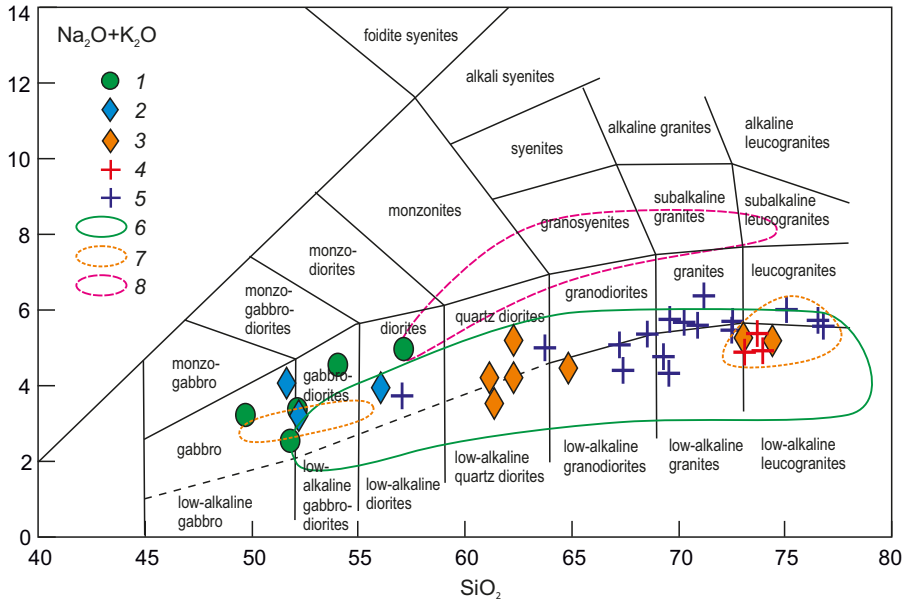

Fig. 4. Diagram (Na_2O+K_2O) – SiO_2 for the Kurmansky massif rocks and magmatic complexes of the region.
1 – gabbro, gabbrodiorites; *2* – microgabbrodiorite dykes; *3* – vein trondhjemites; *4* – trondhjemites of the main phase of the Kurmansky massif; *5* – compositions of granitoids Kurmansky massif, according to [Rapoport, Medyakov, 1974; Kubashin, Lykova, 1985]; *6–8* – field compositions: *6* – gabbro, tonalites, plagiogranites of the Reftinsky complex [Fershtater, 2013; Smirnov et al., 2018], *7* – gabbro and trondhjemites of the Averinsky complex [Lobova, et al., 2012], *8* – granodiorites and granites of the Kamensky complex [Fershtater, 2013]. The points of rock compositions in the diagram are calculated for the dry residue.

Рис. 4. Диаграмма (Na_2O+K_2O) – SiO_2 для пород Курманского массива в сопоставлении с магматическими комплексами района.
1 – габбро, габбро-диориты; *2* – дайки микрогаббро-диоритов; *3* – жильные трондьемиты; *4* – трондьемиты главной фазы Курманского массива; *5* – составы гранитоидов Курманского массива по данным [Rapoport, Medyakov, 1974; Kubashin, Lykova, 1985]; *6–8* – поля составов: *6* – габбро, тоналитов, плагиогранитов рефтинского комплекса [Fershtater, 2013; Smirnov et al., 2018], *7* – габбро и трондьемитов аверинского комплекса [Lobova et al., 2012], *8* – гранодиоритов и гранитов каменского комплекса [Fershtater, 2013]. Точки составов пород на диаграмме рассчитаны на сухой остаток.

(calc-alkaline) rocks whereas gabbro, gabbrodiorites and diorites are located along the separating line between magnesium and ferruginous rock series (Fig. 5). On diagram ($Na_2O+K_2O–CaO$)–SiO_2, the points of trondhjemites fall within the field of calcareous rock series, and those of gabbrodiorites – in the fields of calcareous and calc-alkaline rock series (Fig. 5).

On discriminant diagrams (Fig. 6, a, b), points of gabbro, gabbrodiorites and diorites fall within the fields of island-arc-type rocks. High Th and low Nb contents in gabbroids imply an active participation of slab-derived fluid component in melting of mantle peridotite depleted in trace elements. Trondhjemites are located in the fields of island-arc-type granitoid rocks (Fig. 6, c, b).

5.2. Features of the mineral rock composition

Amphibole. A chemical composition of amphibole in calculating the crystal-chemical ratios per 23 oxygens is characterized by the value of Ca_B=1.7–2.0 и $(Na+K)_A$=0.26–0.45 and the ratio of $Mg/(Mg+Fe^{2+})$=0.56–0.63, which makes it possible to define it as tschermakite in accordance with the nomenclature [Leake at al., 1997] or as amphibole in accordance with [Hawthorne et al., 2012]. Note that the compositions of amphibole in different rocks vary inconsiderably.

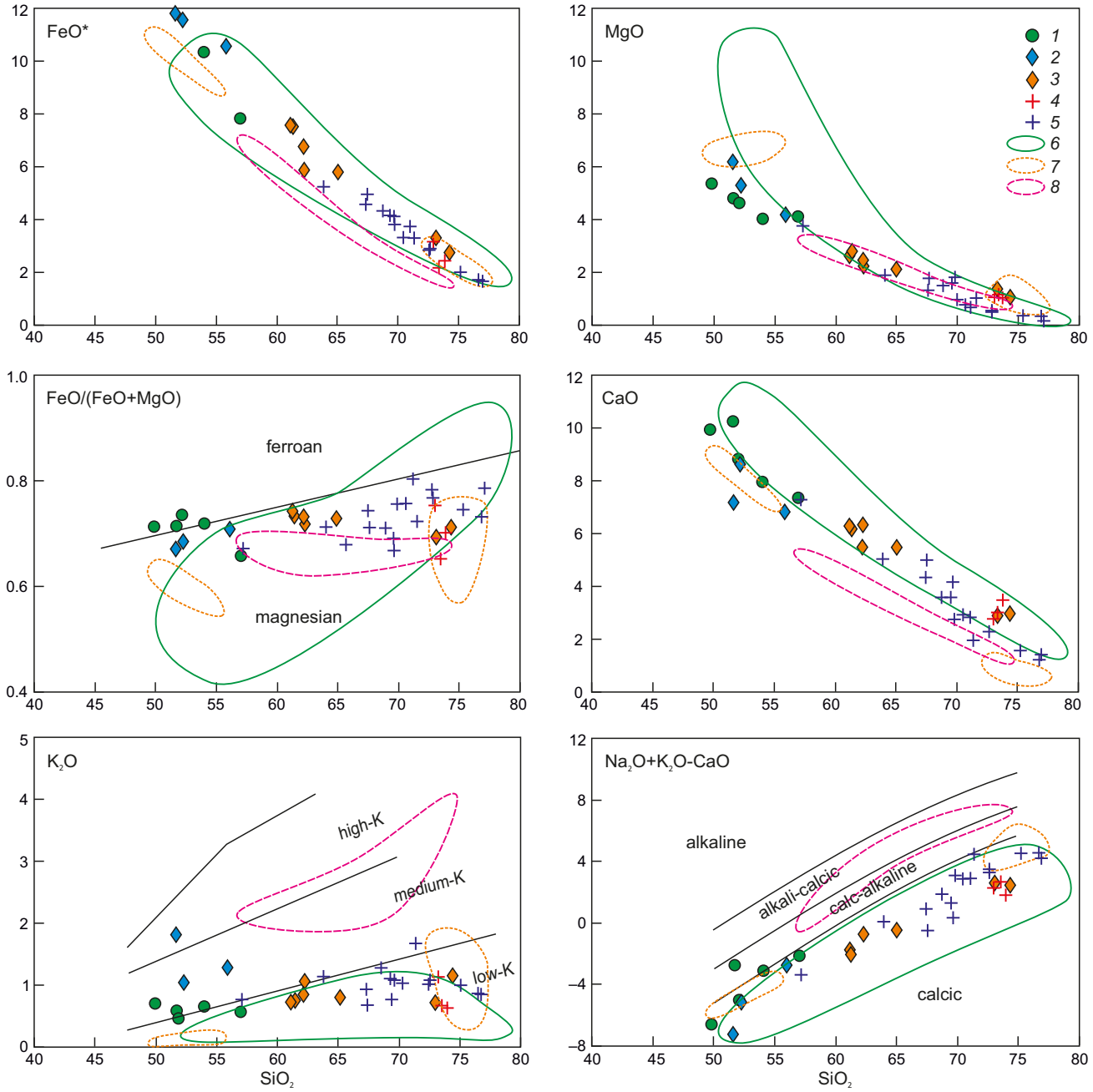

Fig. 5. Diagrams for the Kurmansky massif rocks and magmatic complexes of the region. See the legend in Fig. 4.

Рис. 5. Диаграммы для пород Курманского массива в сопоставлении с магматическими комплексами района. Условные обозначения см. рис. 4.

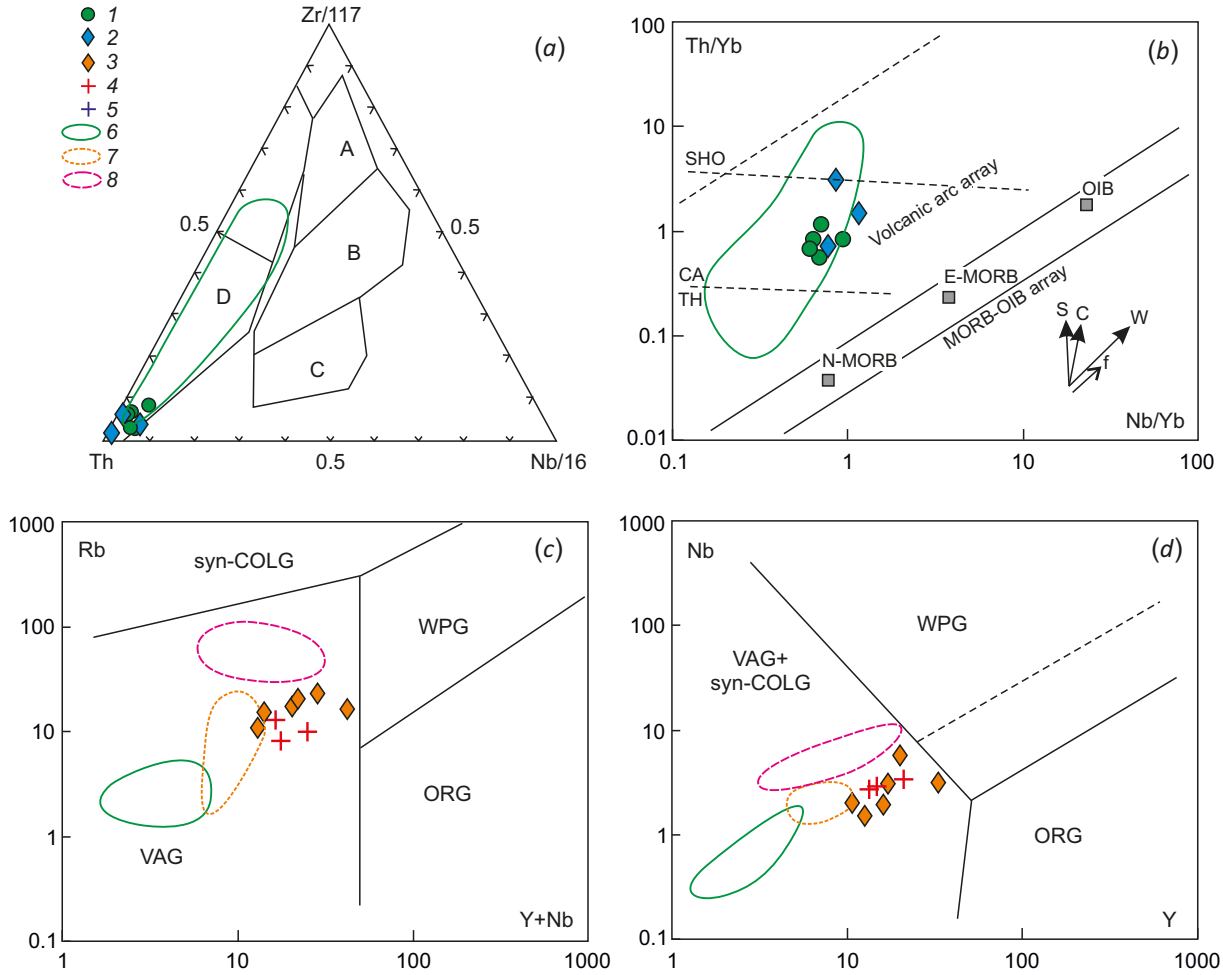

Fig. 6. Geodynamic discriminant diagrams for the Kurmansky massif rocks and magmatic complexes of the region.
(*a*) – diagram Th–Zr/117–Nb/16 [Wood, 1980] for basic rocks. Fields in the diagram: A – mid-ocean ridges; B – basalts of mid-ocean ridges and intraplate settings; C – basalts of intraplate settings; D – basalts of island arcs and active continental margins. (*b*) – diagram of Nb/Yb–Th/Yb [Pearce, 2008] for the basic rocks. Fields: TH – tholeiitic basalts, CA – calc-alkaline basalts, SHO – subalkaline basalts of active continental margins. The arrows show the increasing importance of the subduction component (S), crustal contamination (C), within-plate component (W), and fractional crystallization (f). (*c*), (*d*) – diagrams (Y+Nb)–Rb and Y–Nb for acid rocks [Pearce et al., 1984]. Fields: VAG – granites of volcanic arcs, ColG – syn-collision granites, WPG – intraplate granites, ORG – granites of oceanic ridges. See the legend in Fig. 4.

Рис. 6. Геодинамические дискриминантные диаграммы для пород Курманского массива в сопоставлении с магматическими комплексами района.
(*a*) – диаграмма Th–Zr/117–Nb/16 [Wood, 1980] для основных пород. Поля на диаграмме: A – срединно-океанических хребтов; B – базальты срединно-океанических хребтов и внутриплитных обстановок; C – базальты внутриплитных обстановок; D – базальты островных дуг и активных континентальных окраин. (*b*) – диаграмма Nb/Yb–Th/Yb [Pearce, 2008] для основных пород. Поля на диаграмме: TH – толеитовые базальты, CA – известково-щелочные базальты, SHO – субщелочные базальты активных континентальных окраин. Стрелками показаны тренды возрастания роли субдукционного компонента (S), коровой контаминации (C), внутриплитного компонента (W) и фракционной кристаллизации (f). (*c*), (*d*) – диаграммы (Y+Nb)–Rb и Y–Nb для кислых пород [Pearce et al., 1984]. Поля на диаграммах: VAG – граниты вулканических дуг, Syn-COlG – коллизионные граниты, WPG – внутриплитные граниты, ORG – граниты океанических хребтов. Условные обозначения см. на рис. 4.

The average ferruginosity value (f) of amphibole in gabbro, gabbrodiorites and diorites is 0.47, in trondhjemites – 0.52. The alkali and aluminum content of amphibole in trondhjemites is also somewhat higher. PT-conditions of crystallization for amphibole have been calculated based on the known thermobarometers (App. 1, Table 2) and are 660–690 °C, 7–9 kbar.

Biotite. F of biotite varies from gabbro to trondhjemite within the range of 0.37–0.47. Worthy of note is a decrease in F of biotite relative to amphibole, typical of rocks of abissal level generation and products of water-saturated anatexis [Fershtater, 2013].

Plagioclase. It has already been mentioned that the rocks contain two types of plagioclase which differ in composition: large corroded matrixes containing $An_{30–42}$ in gabbro and $An_{24–25}$ in trondhjemites and small granulomorphic grains which were formed during the recrystallization of the latter. The main feature of granulomorphic plagioclase

is the same composition (An_{20-24}) in all rock types. A few-number increase in the content of anorthite in the grain margins implies increasing pressure and temperature during recrystallization process.

6. DISCUSSION OF RESULTS

6.1. Genesis of original melts of basic and acid composition

Partial melting and fractional crystallization play a leading role in generation of acid melts [Rushmer, 1991; Beard, Lofgren, 1991; Wolf, Wyllie, 1994; Rapp, Watson, 1995; Zharikov, Khodorevskaya, 2006; and others]. The melt compositions obtained through one of these processes follow the corresponding geochemical trends which allow determining one or another process contribution to the genesis of rock series. The assumption that the Kurmansky massif trondhjemites may have resulted from fractional crystallization of basic melts, parent for their associated gabbro, is contradicted by an equal or close ferruginosity value of mafic and felsic rocks and by similar potassium contents in all rock types (see App. 1, Table 1; see Fig. 5). On the contrary, these features may indicate the generation of acid melts as a result of water-saturated melting of hornblende gabbro at the condition of the amphibole stability area as earlier suggested by [Fershtater, 2013] for the Kurmansky massif.

On geochemical diagrams, the main-phase trondhjemites, together with gabbro-intersecting veined trondhjemites, cluster both along the trend of fractional crystallization of basic melt corresponding in composition to the massif gabbro and gabbrodiorite (Fig. 7, a, c) and along the trend of gabbro partial melting (Fig. 7, b). This fact most likely suggests that the initial melts for gabbro and trondhjemite of the massif are genetically unrelated and have different sources, although they were even jointly localized in the crust. Presumably, the process that led to the formation of the massif trondhjemites was melting of amphibolites or hornblende gabbro of the lower crust. Gabbro, gabbrodiorites and diorites are the results from the consistent fractional crystallization of basic magma generated by partial melting of the upper mantle. The reason for mantle melting could be an input of fluid component from the subduction zone, as particularly evidenced by high Ba/Th and low Th/Nb ratios in the rocks (Fig. 8, a). However, high Si, K, Rb, Sr, Ba, La concentrations and increasing Sr/Nb and Gd/Yb ratios in gabbroids (Fig. 8, b) imply melting of peridotites, previously metasomatized, as well as by subduction-related melts with adakite-like geochemical features.

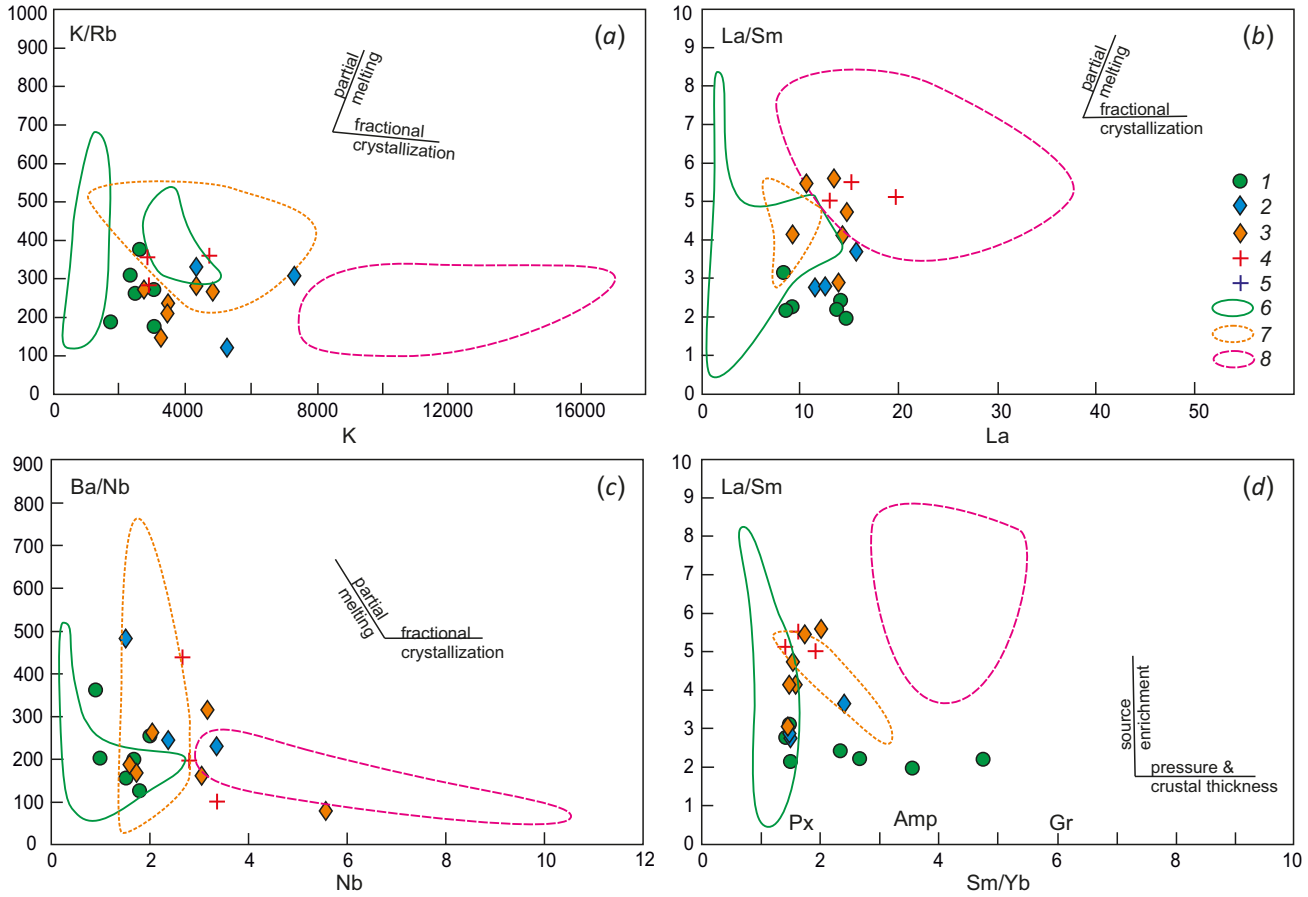

Fig. 7. Diagrams K/Rb – K, La/Sm – La, Ba/Nb – Nb [Bourdon et al., 2002], La/Sm – Sm/Yb [Kay, Mpodozis, 2001; Zarasvandi et al., 2016] for the Kurmansky massif rocks and magmatic complexes of the region. See the legend in Fig. 4.

Рис. 7. Диаграммы K/Rb – K, La/Sm – La, Ba/Nb – Nb [Bourdon et al., 2002], La/Sm – Sm/Yb [Kay, Mpodozis, 2001; Zarasvandi et al., 2016] для пород Курманского массива и магматических комплексов района. Условные обозначения см. на рис. 4.

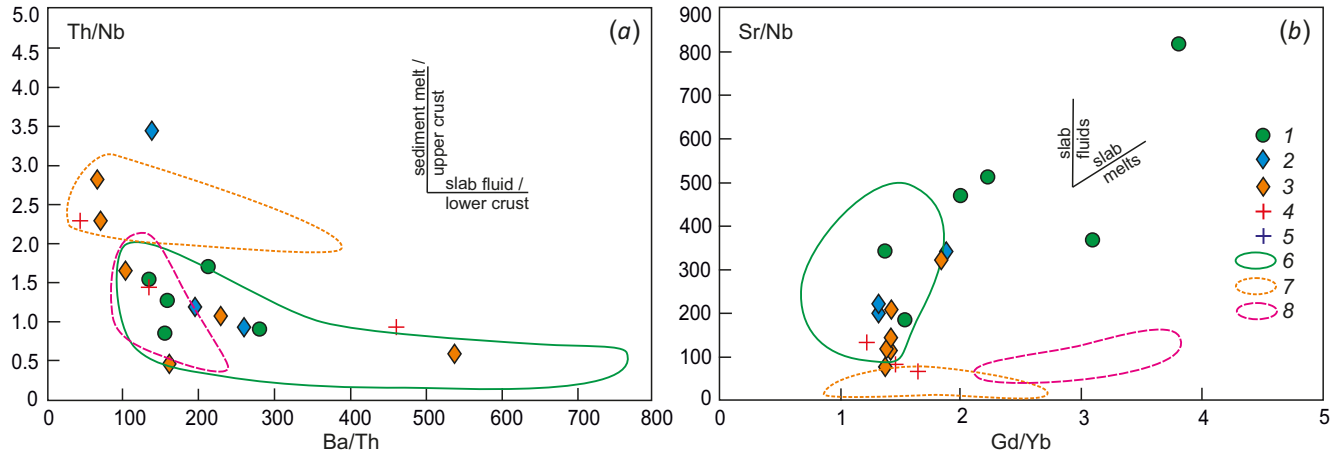

Fig. 8. Diagrams of relations of Th/Nb – Ba/Th [Hanyu et al., 2006] and Sr/Nb – Gd/Yb [Mori et al., 2007] for the Kurmansky massif rocks and magmatic complexes of the region, demonstrating the participation of various crustal components in the metasomatic enrichment of the mantle. See the legend in Fig. 4.

Рис. 8. Диаграммы Th/Nb – Ba/Th [Hanyu et al., 2006] и Sr/Nb – Gd/Yb [Mori et al., 2007] для пород Курманского массива и комплексов района, демонстрирующие участие различных коровых компонентов в метасоматическом обогащении мантии. Условные обозначения см. на рис. 4.

6.2. Conditions of melts separation and crystallization

Low Sr/Y, La/Yb (see App. 1, Table 1), Sm/Yb (see Fig. 7, d) ratios in trondhjemites suggest absence of garnet as a restitic phase during melting of amphibolite source. The absence of garnet, in accordance with [Wolf, Wyllie, 1994; Rapp, Watson, 1995; and others], defines the area of trondhjemite melt separation at a pressure no higher than 9–12 kbar. The ratios of normative components Qz, Ab, An, Or allow estimating the melt crystallization parameters. The position of normative trondhjemite compositions in the system of ternary feldspars [Elkins, Grove, 1990] provides an approximate estimate of the temperature of the beginning of melt crystallization as 700–900 °C (Fig. 9, a). The relationship between the content of normative quartz in melt and the pressure with regard to culculated temperatures defines the position of liquids on PT-diagram. The trondhjemite composition consistency along the lines of constant water content 2–4 % indicates an adiabatic evolution of liquids when they move from the place of their origin at 9–12>P_{tot}≥8 kbar and P_{H_2O}=0.1–0.2P_{tot} in the amphibole (±biotite) stability area to the place of localization and crystallization in the upper crust at P_{tot}=P_{H_2O}=1 kbar.

The development of wollastonite skarns in contact with trondhjemites allows estimating depth of appearance of massif in tht crust level by independent way. It can be determined from the intersection point of reaction paths An+Qz+ +Cc=Grs+CO_2 and Qtz+Cc=Wo+CO_2 for paragenesis of wollastonite associated with grossular depending on CO_2 mole fraction [Schmädicke et al., 2001; Zharikov, Rusinov, 1998]. When CO_2 mole fraction is about 0.2 (typical value for magmatogenic fluid), the minimum pressure in garnet-wollastonite skarn generation will be 1 kbar. Therefore, we can establish the mesoabissal level of the Kurmansky massif.

The reconstruction of initiation, evolution and crystallization conditions of gabbro, gabbrodiorite and diorite melts in the massif is a much more complicated task. Nevertheless, the position of gabbro composition points close to eutectic An – Cpx – Opx at 10 kbar, calculated for the bodies with f=0.6 (Fig. 9, c), implies the separation of basic calc-alkaline melt at the upper mantle level. The positions of points of microgabbro and microdiorite dykes follow the isobaric trend in the evolution of gabbroids.

6.3. Rock metamorphism

The development of micro-grained and fine-grained quartz-feldspar aggregate in all massif rocks indicates the occurrence of high-temperature recrystallization (metamorphism) associated with granulation, grain misorientation and plagioclase deanorthitization. Recrystallization also gave rise to the appearance of epidote, scurfy biotite and amphibole. The latter probably formed by the primary gabbroid pyroxene that is responsible for its low alkalinity. The parameters calculated for recrystallization, in accordance with App. 1, Table 2, correspond to the upper epidote-amphibolite facies (7–9 kbar and 670–690 °C), which does not exclude the melting of the most easily fusible rocks with occurrence of migmatite zones along the fluid channels. Relatively high parameters of rock metamorphism may result from their occurrence in the bottom of the allochtonous block. Microstructures structures similar to hornfelsic ones that form under high pressure may be attributed to transformation of stress pressure into normal hydrostatic pressure for competent rock blocks in thrust zones [Kozlovsky, Viryus, 2011; Kulakovsky et al., 2015].

6.4. Rock dating problem

An important and still ambiguously unsolvable problem is the time of placement of massif in the crust. The U-Pb age of zircons from gabbro and trondhjemite (411–397 Ma) [Fershtater, 2013, 2015] were interpreted as a span of magmatic crystallization of the rocks.

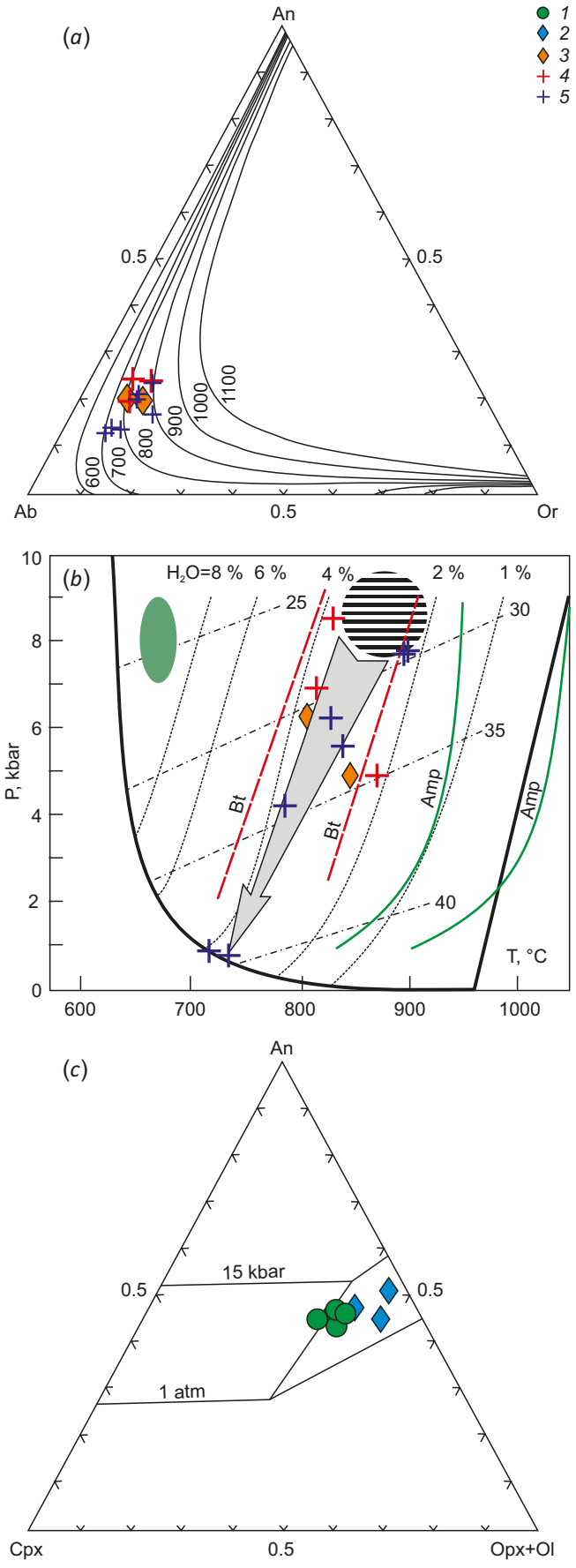

Fig. 9. PT-conditions of melting, crystallization and metamorphism for the Kurmansky massif trondhjemites.
See the legend in Fig. 4. (*a*) – triangular diagram An – Ab – Or for granite compositions. Normative quantities of An, Ab, Or are calculated by CIPW; isotherms are calculated on the basis of a triple feldspar model for 8 kbar [Elkins, Grove, 1990]. (*b*) – PT-diagram of the evolution of trondhjemite melts. Thick solid lines – dry and wet liquiduses of granite melt, thin dotted lines – water content (wt. %) [Johannes, Holtz, 1996], dashed lines – the content of normative quartz in the Qtz – Or – Ab system [Fershtater, 1987, Fig. 33], dotted red and solid green lines are the stability lines of biotite and amphibole according to different authors [Yoder, Tilley, 1962; Wyllie, Wolf, 1993; Weinberg, Hasalova, 2015, and references therein]. The horizontal hatching shows the area of origin of trondjemite melts, and the arrow shows the trend of their magmatic evolution. Trondhjemite points are plotted in accordance with the content of normative quartz in the rock and the temperature of the feldspar solvus. The green field is the area of metamorphism of gabbro and trondhjemites in accordance with the data [HB] of App. 1, Table 2. (*c*) – triangular diagram Cpx – An – Opx for basites. Green circles and blue rhombuses indicate the compositions of gabbro, gabbrodiorites, and diorites of the massif. The An – Cpx – Opx cotectics are calculated for compositions with a Fe/Fe+Mg=0.6 at 1 atm and 15 kbar. See [Fershtater, 1987] for the method of the diagram construction.

Рис. 9. PT-условия плавления, кристаллизации и метаморфизма трондьемитов Курманского массива.
Условные обозначения см. на рис. 4. (*a*) – диаграмма An – Ab – Or для гранитных составов. Нормативные количества An, Ab, Or рассчитаны методом CIPW; изотермы – на основе тройной модели полевого шпата для 8 кбар [Elkins, Grove, 1990]. (*b*) – PT-диаграмма эволюции трондьемитовых расплавов. Толстые сплошные линии – сухой и мокрый ликвидусы гранитного расплава, тонкие пунктирные линии – содержания воды (мас. %) [Johannes, Holtz, 1996], штрихпунктирные линии – содержания нормативного кварца в системе Qtz – Or – Ab [Fershtater, 1987, рис. 33], пунктирные красные и сплошные зеленые линии – линии стабильности биотита и амфибола по разным авторам [Yoder, Tilley, 1962; Wyllie, Wolf, 1993; Weinberg, Hasalová, 2015, и ссылки в ней]. Горизонтальной штриховкой показана область зарождения трондьемитовых расплавов, а стрелкой – тренд их магматической эволюции. Точки трондьемитов нанесены в соответствии с содержанием нормативного кварца в породе и значением температуры полевошпатового сольвуса. Зеленое поле – область метаморфизма габбро и трондьемитов в соответствии с данными [HB] Прил. 1, табл. 2. (в) – диаграмма Cpx – An – Opx для базитов. Зелеными кружками и синими ромбами указаны составы габбро, габбро-диоритов, диоритов массива. Котектики An – Cpx – Opx рассчитаны для составов с железистостью 0.6 при 1 атм и 15 кбар. Методику построения диаграммы см. в работе [Fershtater, 1987].

The lack of data about validity (MSWD values) of these ages and the existence of metamorphic transformations of the rocks suggest an incomplete correspondence between zircon isotope ages and a time span of their magmatic crystallization. Such datings most likely fall within the time of magmatic crystallization (430–420 Ma) of the rocks consisting of the main part of the Reftinsky allochthone, and the age of their metamorphism (405–380 Ma). The last event was caused by accretion and thrusting of the O-S oceanic and S-D island arc complexes of the Reftinsky allochthone on the Murzinsky-Aduysky terrain in the Late Devonian [Smirnov et al., 2014].

6.5. Comparison with magmatic complexes of the East Uralian megazone

According to [Puchkov, 2000; Smirnov et al., 2003; Smirnov, Korovko, 2007; and others], the most ancient rocks in the area are ophiolites of dunite-harzburgite-gabbro and volcanic rock of basalt-dacite and basalt-andesite-dacite complexes with their supposedly co-magmatic intrusions of the Silurian and Early Devonian (?) ages. After the formation of thick Silurian volcanic suites, the magmatic activity of the area decreased and then terminated in low part of the Early Devonian, so the formation of thick carbonate and terrigenous-carbonate suites took place during the Late Silurian to Middle Devonian. New impulse of magmatic activity caused the generation of volcano-plutonic complexes containing xenoliths of the Silurian volcanites and Early Devonian limestones from the basement.

Taking into account ambiguity in the Kurmansky massif rock dating, we made a comparison between the rock composition and the most accurately dated and intrusive complexes of the area whose geochemistry has been well studied. The materials compared were Reftinsky gabbro-diorite-tonalite-plagiogranite (435–430 Ma) and Averinsky diorite-trondhjemite (420–419 Ma) complexes of the island arc nature [Lobova et al., 2012; Fershtater, 2013; Smirnov et al., 2014, 2018] wherein the Kurmansky massif was also localized (see Fig. 1). Separate comparison was made between the Kurmansky trondhjemites and the early-collisional Kamensky granodiorite complex (298–309 Ma) [Fershtater, 2013], since Kurmansky massif was arbitrarily assigned to this complexon the latest State Geological Map [State Geological Map..., 2017].

The rocks of the Reftinsky complex (gabbro, tonalites, plagiogranites) preceding magmatites of the Kurmansky massif have similarly low contents of K, Rb, Sr, Ba, RE and REE, and their formation is related to low baric partial melting of the upper mantle and basic crust at the island arc stage with the slab-fluid component participating in magma generation (see Figs. 7, 8). This is evidenced by the results of the isotope study of Sr, Nd, Hf in the rocks of the Reftinsky complex [Smirnov et al., 2018]. Probably, an increasing importance of the slab-related fluid (±acidic melt) providing an effect of metasomatism to the magmogenerated sources in the upper mantle and crust might have further determined the generation of melts more enriched in Sr, Ba, Rb and REE, similar to the Kurmansky gabbroids. The differences in Y, Sr, Cr, Ni and Co contents imply the belonging of the Reftinsky gabbro to the ophiolite associations, and that of the Kurmansky gabbro to the gabbro-granite series (after [Ferstater, 1987]).

The trondhjemites (now blastomilonites) of the Averinsky complex adjacent to the Kurmansky massif in the east have a clearly defined negative Eu-anomaly and lower REE contents. Besides, they have a high Al-content (A/CNK= =1.2–1.5 [Lobova et al., 2012] against 0.64–0.79 in the Kurmansky massif rocks). These data imply different sources for the Averinsky and Kurmansky trondhjemites.

A preliminary attribution of rocks of the Kurmansky massif to the Kamensky complex [State Geological Map..., 2017] seems unreasonable, since rocks of these objects have a different ages and they form quite individual series having different contents of main and trace elements (see Figs. 4, 5, 6, 7, 8).

The results of comparison between the compositions of the rocks in the Kurmansky massif and the major rock series from the considered sector of the Middle Uralian area of the East Uralian megazone, we propose to allocate the Early Devonian (?) Kurmansky gabbro-diorite-trondhjemite island arc complex as an individual subdivision.

7. CONCLUSION

The generation of the Kurmansky gabbro-trondhjemite massif is related to the last stages of the Silurian – Early Devonian island-arc magmatism in the East Uralian megazone accompanied by processes of partial melting of the upper mantle and crust which were brought together in time and space. The mantle peridotites that melt partially under the effect of aqueous fluids released from the subduction zone were the sources for the gabbro melts. Such melts were separated and followed two-pyroxene plagioclase cotectics at P=10 bar. Partial melting of amphibolites or amphibole gabbro in the lower crust at $P_{tot} \geq 8$ kbar P_{H_2O}= =0.1–0.2 P_{tot} caused the generation of initial trondhjemite melts. The crystallization of basic and acid rocks of the massif ceased at the mesoabyssal conditions at $P_{tot}=P_{H_2O}=1$ kbar and accompanied by the formation of wollastonite scarns at the contacts between limestones and trondhjemites. This interpretation of genesis and crystallization conditions of the massif rocks differs from the earlier version [Fershtater, 2013].

The age, geological-structural position and features of composition of the rocks in the Kurmansky massif (in a specified volume) provide evidence for its belonging to the individual Early Devonian (?) magmatic complex of the island-arc origin.

The generation of the rocks in the Kurmansky massif and their metamorphic transformations might have been caused by temporally convergent processes of magmatism and accretion of the Early Paleozoic – Early Devonian complexes on the Murzinsky-Aduysky terrain during the Devonian. The appearance of hornfels-like microstructures formed under conditions of the epidote-amphibolite facies at the medium pressures is the characteristic feature of metamorphism of the Kurmansky massif rocks.

8. ACKNOWLEDGEMENTS

The authors express their sincere gratitude to V.I. Kvachev for data collection assistance, and to N.S. Borodina, E.V. Pushkarev, G.Yu. Shardakova and V.N. Smirnov for constructive discussions of the results obtained.

9. CONTRIBUTION OF THE AUTHORS

The authors contributed equally to this article.

Все авторы внесли эквивалентный вклад в подготовку публикации.

10. CONFLICT OF INTERESTS

The authors have no conflicts of interest to declare. All authors have read and agreed to the published version of the manuscript.

Авторы заявляют об отсутствии у них конфликта интересов. Все авторы прочитали рукопись и согласны с опубликованной версией.

11. REFERENCES

Beard J.S., Lofgren G.E., 1991. Dehydration Melting and Water-Saturated Melting of Basaltic and Andesitic Greenstones and Amphibolites at 1.3 and 6.9 Kb. Journal of Petrology 32 (2), 365–402. https://doi.org/10.1093/petrology/32.2.365.

Blundy J., Holland T.J., 1990. Calcic Amphibole Equilibria and a New Amphibole-Plagioclase Geothermometer. Contributions to Mineralogy and Petrology 104, 208–224. https://doi.org/10.1007/BF00306444.

Bourdon E., Eissem J.-P., Monzier M., Robin C., Martin H., Cotton J., Hall M.L., 2002. Adakite-like Lavas from Antisana Volcano (Ecuador): Evidence for Slab Melt Metasomatism beneath the Andean Northern Volcanic Zone. Journal of Petrology 43 (2), 199–217. https://doi.org/10.1093/petrology/43.2.199.

Elkins L.T., Grove T.L., 1990. Ternary Feldspar Experiments and Thermodynamic Models. American Mineralogist 75 (5–6), 544–559.

Eselevich L.V., Sergievskaya N.V., 1953. Geological Report on the Results of the Work of the Bazhenov Field Party over the Period of 1949–1952. Ural Geological Survey Expedition, Sverdlovsk (in Russian) [Еселевич Л.В., Сергиевская Н.В. Геологический отчет о результатах работ Баженовской ГРП за 1949–1952 гг. Свердловск: УКСЭ, 1953].

Fershtater G.B., 1987. Petrology of Major Intrusive Associations. Nauka, Moscow, 231 p. (in Russian) [Ферштатер Г.Б. Петрология главных интрузивных ассоциаций. М.: Наука, 1987. 231 с.].

Fershtater G.B., 1990. Empirical Hornblende-Plagioclase Geobarometer. Geochemistry 3, 328–335 (in Russian) [Ферштатер Г.Б. Эмпирический плагиоклаз-роговообманковый барометр // Геохимия. 1990. № 3. С. 328–335].

Fershtater G.B., 2013. Paleozoic Intrusive Magmatism of the Middle and South Urals. Publishing House of the Ural Branch of RAS, Ekaterinburg, 368 p. (in Russian) [Ферштатер Г.Б. Палеозойский интрузивный магматизм Среднего и Южного Урала. Екатеринбург: Изд-во УрО РАН, 2013. 368 с.].

Fershtater G.B., 2015. Early Devonian Intrusive Magmatism of the Urals as Indicator Critical Stage Paleozoic History Mobile Belt. Lithosphere 5, 5–29 (in Russian) [Ферштатер Г.Б. Раннедевонский интрузивный магматизм Урала – индикатор переломного этапа в палеозойской истории подвижного пояса // Литосфера. 2015. № 5. С. 5–29].

Fershtater G.B., Borodina N.S., Bea F., Montero P., 2018. Model of Mantle-Crust Interaction and Magma Generation in the Suprasubduction Orogen (Paleozoic of the Urals). Lithosphere 18 (2), 177–207 (in Russian) [Ферштатер Г.Б., Бородина Н.С., Беа Ф., Монтеро П. Модель мантийно-корового взаимодействия и сопряженного магматизма в надсубдукционном орогене (палеозой Урала) // Литосфера. 2018. Т. 18. № 2. С.177–207]. https://doi.org/10.24930/1681-9004-2018-18-2-177-207.

Frost B.R., Arculus R.J., Barnes C.G., Collins W.J., Ellis D.J., Frost C.D., 2001. A Geochemical Classification of Granitic Rocks. Journal of Petrology 42 (11), 2033–2048. https://doi.org/10.1093/petrology/42.11.2033.

Hanyu T., Tatsumi Y., Nakai S., Chang Q., Miyazaki T., Sato K., Tani K., Shibata T., Yoshida T., 2006. Contribution of Slab Melting and Slab Dehydration to Magmatism in the NE Japan Arc for the Last 25 Myr: Constraints from Geochemistry. Geochemistry, Geophysics, Geosystems 7 (8). https://doi.org/10.1029/2005GC001220.

Hawthorne F.C., Oberti R., Harlow G.E., Maresch W.V., Martin R.F., Schumacher J.C., Welch M.D, 2012. Nomenclature of the Amphibole Supergroup. American Mineralogist 97 (1–2), 2031–2048. https://doi.org/10.2138/am.2012.4276.

Holland T.J., Blundy J., 1994. Non-Ideal Interactions in Calcic Amphiboles and Their Bearing on Amphibole-Plagioclase Thermometry. Contributions to Mineralogy and Petrology 116, 433–447. https://doi.org/10.1007/BF00310910.

Johannes W., Holtz F., 1996. Petrogenesis and Experimental Petrology of Granitic Rocks. Springer-Verlag, Berlin, Heidelberg, 335 p. https://doi.org/10.1007/978-3-642-61049-3.

Kay S.M., Mpodozis C., 2001. Central Andean Ore Deposits Linked to Evolving Shallow Subduction Systems and Thickening Crust. Geological Society of America Today 11, 4–9. https://doi.org/10.1130/1052-5173(2001)011<0004:CAODLT>2.0.CO;2.

Kozlovsky V.M., Viryus A.A., 2011. Granulite Parageneses in Local Deformation Zones of the Eastern Belomorye. In: Granulite and Eclogite Complexes in the History of the Earth. Proceedings of Scientific Conference and Scientific Excursion Guide (June 16–18, 2011). KarRC RAS, Petrozavodsk, p. 93–97 (in Russian) [Козловский В.М., Вирюс А.А. Гранулитовые парагенезисы в локальных зонах деформаций Восточного Беломорья // Гранулитовые и эклогитовые комплексы в истории Земли: Материалы научной конференции и путеводитель научных экскурсий (16–18 июня 2011 г.). Петрозаводск: КарНЦ РАН, 2011. С. 93–97].

Kubashin N.N., Lykova V.V., 1985. Geological Report on the Results of Further Exploration and Reassessment of the Kurmanskii Building Stone Deposit (Further Exploration of Deep Horizons of the Active Quarry) Conducted in 1982–1985 in the Beloyarsky District, Sverdlovsk Oblast, with the Calculation of Recourses as at 01.01.1986. Middle-Ural Geological Expedition, Verkhnyaya Pyshma (in Russian) [Кубашин Н.Н., Лыкова В.В. Геологический отчет о результатах доразведки и переоценки Курманского месторождения строительного камня (доразведка глубоких горизонтов действующего карьера), произведенной в 1982–1985 гг. в Белоярском районе Свердловской области с подсчетом запасов по состоянию на 01.01 1986 года. В. Пышма: СУГРЭ, 1985].

Kulakovsky A.L., Morozov Yu.A., Smul'skaya A.I., 2015. Tectonic Stress as Additional Termodynamic Factor of Metamorphism (Northern Ladoga Region). Geophysical Research 16 (1), 44–68 (in Russian) [Кулаковский А.Л., Морозов Ю.А., Смульская А.И. Тектонический стресс как дополнительный термодинамический фактор метаморфизма // Геофизические исследования. 2015. Т. 16. № 1. С. 44–68].

Leake B., Woolley A., Arps C., Birch W., Gilbert C., Grice J., Hawthorne F., Kato A. et al., 1997. Nomenclature of Amphiboles; Report of the Subcommittee on Amphiboles of the International Mineralogical Association Commission on New Minerals and Mineral Names. Mineralogical Magazine 61 (405), 295–310. https://doi.org/10.1180/minmag.1997.061.405.13.

Lobova E.V., Smirnov V.N., Bayanova T.B., 2012. Averinskyi Diorite-Trodhjemite Complex, Eastern Zone of the Middle Ural. Lithosphere 3, 49–64 (in Russian) [Лобова Е.В., Смирнов В.Н., Баянова Т.Б. Аверинский диорит-трондьемитовый комплекс восточной зоны Среднего Урала // Литосфера. 2012. № 3. 49–64].

Mori L., Gómez-Tuena A., Cai Y., Goldstein S.L., 2007. Effects of Prolonged Flat Subduction on the Miocene Magmatic Record of the Central Trans-Mexican Volcanic Belt. Chemical Geology 244 (3–4), 452–473. https://doi.org/10.1016/j.chemgeo.2007.07.002.

Pearce J.A., 2008. Geochemical Fingerprinting of Oceanic Basalts with Applications to Ophiolite Classification and the Search for Archean Oceanic Crust. Lithos 100 (1–4), 14–48. https://doi.org/10.1016/j.lithos.2007.06.016.

Pearce J.A., Harris N.B.W., Tindle A.G., 1984. Trace Element Discrimination Diagrams for the Tectonic Interpretation of Granitic Rocks. Journal of Petrology 25 (4), 956–983. https://doi.org/10.1093/petrology/25.4.956.

Pribavkin S.V., Zamyatina M.D., Zamyatin D.A., Gulyaeva T.Ya., Kvachev V.I., 2014. Wollastonite Scarns and Associated Cu-Pb-Bi-Mineralization of the Kurmanskii Quarry. In: Informational Collection of Scientific Papers of IGG UB RAS. Yearbook 2013. Vol. 161. IGG UB RAS Publishing House, Ekaterinburg, p. 285–289 (in Russian) [Прибавкин С.В., Замятина М.Д., Замятин Д.А., Гуляева Т.Я., Кварчёв В.И. Волластонитовые скарны и сопутствующая Cu–Pb–Bi-минерализация Курманского карьера // Информационный сборник научных трудов ИГГ УрО РАН. Ежегодник-2013. Екатеринбург: Изд-во ИГГ УрО РАН, 2014. Вып. 161. С. 285–289].

Puchkov V.N., 2000. Paleogeodynamics of the Southern and Middle Urals. Gilem, Ufa, 146 p. (in Russian) [Пучков В.Н. Палеогеодинамика Южного и Среднего Урала. Уфа: Гилем, 2000. 146 с.].

Rapoport M.S., Medyakov I.A., 1974. Geological Map of the Urals. Scale 1:50000. Sheets O-41-99-Г, O-41-111-Б, O-41-111-Г. Report of the Beloyarsky Geological Survey Party on Further Geological Studies over the Period of 1970–1974. Ural Geological Survey Expedition, Sverdlovsk (in Russian) [Рапопорт М.С., Медяков И.А. Геологическая карта Урала масштаба 1:50000. Листы O-41-99-Г. O-41-111-Б. O-41-111-Г. Отчет Белоярского геологосъемочного отряда о геологическом доизучении за 1970–1974 гг. Свердловск: УКСЭ, 1974].

Rapp R.P., Watson E.B., 1995. Dehydration Melting of Metabasalt at 8–32 Kbar: Implications for Continental Growth and Crust-Mantle Recycling. Journal of Petrology 36 (4), 891–931. https://doi.org/10.1093/petrology/36.4.891.

Rushmer T., 1991. Partial Melting of Two Amphibolites: Contrasting Experimental Results under Fluid Absent Conditions. Contributions to Mineralogy and Petrology 107, 41–59. https://doi.org/10.1007/BF00311184.

Schmädicke E., Okrusch M., Schubert W., Elwart B., Görke U., 2001. Phase Relations of Calc-Silicate Assemblages in the Auerbach Marble, Odenwald Crystalline Complex, Germany. Mineralogy and Petrology 72, 77–111. https://doi.org/10.1007/s007100170028.

Schmidt M.W., 1992. Amphibole Composition in Tonalite as a Function of Pressure: An Experimental Calibration of the Al-in-Hornblende Barometer. Contributions to Mineralogy and Petrology 110, 304–310. https://doi.org/10.1007/BF00310745.

Smirnov V.N., Fershtater G.B., Ivanov K.S., 2003. The Scheme of the Tectonic-Magmatic Zonation of the Eastern Slope of the Middle Urals. Lithosphere 2, 45–56 (in Russian) [Смирнов В.Н., Ферштатер Г.Б., Иванов К.С. Схема тектоно-магматического районирования территории восточного склона Среднего Урала // Литосфера. 2003. № 2. С. 45–56].

Smirnov V.N., Ivanov K.S., Ronkin Y.L., Serov P.A., Gerdes A., 2018. Sr, Nd, and Hf Isotope Composition of Rocks of the Reft Gabbro-Diorite-Tonalite Complex (Eastern Slope of the Middle Urals): Petrological and Geological Implications. Geochemistry International 56 (6), 495–508. https://doi.org/10.1134/S0016702918060101.

Smirnov V.N., Ivanov K.S., Travin A.V., 2019. $^{40}Ar/^{39}Ar$ Age of Rock Deformations across the Bazhenov Suture Zone (Eastern Border of the Middle Urals). Lithosphere 19 (2), 242–249 (in Russian) [Смирнов В.Н., Иванов К.С., Травин А.В. $^{40}Ar/^{39}Ar$ возраст деформаций пород в Баженовской шовной зоне (восточная окраина Среднего Урала) // Литосфера. 2019. Т. 19. № 2. С. 242–249]. https://doi.org/10.24930/1681-9004-2019-19-2-242-249.

Smirnov V.N., Korovko A.V., 2007. Paleozoic Volcanism of the Eastern Middle Urals. In: N.P. Jushkin, V.N. Sazonov (Eds), Geodynamics, Magmatism, Metamorphism, and Ore

Formation. Collection of Scientific Papers. Publishing House of IGG UB RAS, Ekaterinburg, p. 395–420 (in Russian) [Смирнов В.Н., Коровко А.В. Палеозойский вулканизм Восточной зоны Среднего Урала // Геодинамика, магматизм, метаморфизм и рудообразование: Сборник научных трудов / Ред. Н.П. Юшкин, В.Н. Сазонов. Екатеринбург: Изд-во ИГГ УрО РАН, 2007. С. 395–420].

Smirnov V.N., Nastavko E.V., Ivanov K.S., Bayanova T.B., Rodionov N.V., Serov P.A., 2014. The Results of Isotopic Dating of Rocks of the Reftinsky Gabbro-Diorite-Tonalite Complex, Eastern Zone of the Middle Urals. Lithosphere 5, 3–18 (in Russian) [Смирнов В.Н., Наставко Е.В., Иванов К.С., Баянова Т.Б., Родионов Н.В., Серов П.А. Результаты изотопного датирования пород Рефтинского габбро-диорит-тоналитового комплекса. Восточная зона Среднего Урала // Литосфера. 2014. № 5. С. 3–18].

State Geological Map of the Russian Federation, 2015. Middle Urals Series. Scale 1:200000. Sheet O-41-XXXII (Kamensk Area). Explanatory Note. Moscow Branch of VSEGEI, Moscow, 274 p. (in Russian) [Государственная геологическая карта Российской Федерации. Серия Среднеуральская. Масштаб 1:200000. Лист O-41-XXXII (Каменская площадь): Объяснительная записка. М.: МФ ВСЕГЕИ, 2015. 274 с.].

State Geological Map of the Russian Federation, 2017. Middle Ural Series. Scale 1:200000. Sheet O-41-XXVI (Asbest). Explanatory Note. VSEGEI Publishing House, Saint Petersburg, 284 p. (in Russian) [Государственная геологическая карта Российской Федерации. Серия Среднеуральская. Масштаб 1:200000. Лист O-41-XXVI (Асбест): Объяснительная записка. СПб.: ВСЕГЕИ, 2017. 284 с.].

State Geological Map of the USSR, 1987. Scale 1:200000. Middle Ural Series. Sheet O-41-XXVI. Explanatory Note. Uralgeologiya, Sverdlovsk, 162 p. (in Russian) [Государственная геологическая карта СССР. Серия Среднеуральская. Масштаб 1:200000. Лист O-41-XXVI: Объяснительная записка. Свердловск: Уралгеология, 1987. 162 с.].

Weinberg R.F., Hasalová P., 2015. Water-Fluxed Melting of the Continental Crust: A Review. Lithos 212–215, 158–188. https://doi.org/10.1016/j.lithos.2014.08.021.

Wolf M.B., Wyllie P.J., 1994. Dehydration-Melting of Amphibolite at 10 Kbar: The Effects of Temperature and Time. Contributions to Mineralogy and Petrology 115, 369–383. https://doi.org/10.1007/BF00320972.

Wood D.A., 1980. The Application of a Th Hf Ta Diagram to Problems of Tectonomagmatic Classification and to Establishing the Nature of Crustal Contamination of Basaltic Lavas of the British Tertiary Volcanic Province. Earth and Planetary Science Letters 50 (1), 11–30. https://doi.org/10.1016/0012-821X(80)90116-8.

Wyllie P.J., Wolf M.B., 1993. Amphibolite Dehydration-Melting: Sorting Out the Solidus. Geological Society of London Special Publications 76 (1), 405–416. http://dx.doi.org/10.1144/GSL.SP.1993.076.01.20.

Yagovkin V.S., Podkopaeva A.Ya., 1985. Report on Further Exploration of the Kurmanskii Building Stone Deposit in 1964. Ural Geological Survey Expedition, Sverdlovsk (in Russian) [Яговкин В.С., Подкопаева А.Я. Отчет о геологоразведочных работах по доразведке Курманского месторождения строительного камня в 1964 г. Свердловск: УКСЭ, 1985].

Yoder H.S., Tilley C.E., 1962. Origin of Basalt Magmas: An Experimental Study of Natural and Synthetic Rock Systems. Journal of Petrology 3 (3), 342–532. https://doi.org/10.1093/petrology/3.3.342.

Zamyatina M.D., Borodina N.S., 2015. Conditions of the Rocks Formation of the Kurmansky Gabbro-Trondhjemite Massif (The Middle Ural). In: I.I. Chajkovskij (Ed.), The Problems of Mineralogy, Petrography and Metallogeny. Scientific Readings in the Memory of P.N. Chirvinsky. Vol. 18. Publishing House of Perm State University, Perm, p. 167–174 (in Russian) [Замятина М.Д., Бородина Н.С. Условия формирования пород Курманского габбро-трондьемитового массива // Проблемы минералогии, петрографии и металлогении: Научные чтения памяти П.Н. Чирвинского / Ред. И.И. Чайковский. Пермь: Изд-во ПГНИУ, 2015. Вып. 18. С. 167–174].

Zarasvandi A., Rezaei M., Sadeghi M., Lentz D., Adelpour M., Pourkaseb H., 2016. Rare Earth Element Signatures of Economic and Sub-Economic Porphyry Copper Systems in Urumieh–Dokhtar Magmatic Arc (UDMA), Iran. Ore Geology Reviews 70, 407–423. https://doi.org/10.1016/j.oregeorev.2015.01.010.

Zharikov V.A., Khodorevskaya L.I., 2006. Generation of Granites after Amphibolites. Petrology 14, 319–336. https://doi.org/10.1134/S0869591106040011.

Zharikov V.A., Rusinov V.L. (Eds), 1998. Metasomatism and Metasomatic Rocks. Nauchny Mir, Moscow, 492 (in Russian) [Метасоматизм и метасоматические породы / Ред. В.А. Жариков, В.Л. Русинов. М.: Научный мир, 1998. 492 с.].

Table 1. Chemical composition (wt. %) and content of trace elements (ppm) in the rocks of the Kurmanka massif
Таблица 1. Химический состав (мас. %) и содержание малых элементов (г/т) в породах Курманского массива

Sl, No.	1	2	3	4	5	6	7	8	9	10	11	12	13	14	15	16	17	18
SMP No.	Ку-4	413	427	Ку-6б	Ку-5	401	407	404-1	492	404-2	403	Ку-1	408	428	Ку-6а	412	Ку-2	Ку-3
SiO_2	48.84	50.69	50.95	52.71	55.97	50.40	51.14	54.48	59.68	59.92	61.03	61.20	64.85	72.55	73.88	71.50	72.38	72.95
TiO_2	0.86	0.70	0.66	0.89	0.65	0.73	0.67	0.66	0.48	0.49	0.55	0.39	0.44	0.29	0.38	0.36	0.32	0.33
Al_2O_3	16.09	16.97	16.37	17.05	16.97	16.37	17.21	16.92	16.59	17.08	17.27	16.72	16.13	13.18	12.62	14.03	13.74	13.32
Fe_2O_3	9.61	11.77	8.80	4.98	4.64	12.33	11.32	10.30	7.40	7.35	6.64	4.53	5.67	3.02	2.45	3.13	1.35	2.07
FeO	4.60	–	4.60	5.60	3.50	–	–	–	–	–	–	1.70	–	0.50	0.50	–	0.90	0.50
MnO	0.16	0.13	0.16	0.19	0.12	0.17	0.16	0.12	0.09	0.09	0.12	0.09	0.07	0.04	0.07	0.08	0.02	0.02
MgO	5.29	4.70	4.51	3.89	3.99	6.04	5.20	4.14	2.57	2.68	2.44	2.22	2.10	1.44	1.10	1.01	1.14	1.00
CaO	9.77	10.03	8.62	7.76	7.25	7.03	8.51	6.64	6.13	6.06	5.41	6.23	5.44	2.88	3.00	2.78	3.01	3.44
Na_2O	2.67	2.30	3.36	4.20	4.63	2.60	2.60	2.80	3.70	3.10	3.40	4.57	4.00	4.78	4.36	3.90	4.96	4.53
K_2O	0.70	0.60	0.42	0.65	0.56	1.76	1.05	1.27	0.73	0.76	1.05	0.84	0.84	0.71	1.15	1.14	0.69	0.65
P_2O_5	0.35	0.23	0.15	0.20	0.39	0.17	0.11	0.13	0.15	0.13	0.15	0.22	0.11	0.07	0.13	0.07	0.12	0.14
ImPs	0.90	0.54	1.10	0.90	0.70	0.74	0.28	0.60	1.06	1.00	0.18	0.70	0.25	0.50	0.40	0.24	0.50	0.30
Total	99.84	98.66	99.7	99.02	99.37	98.34	98.25	98.06	98.58	98.66	98.24	99.41	99.9	99.96	100.04	98.24	99.13	99.25
Li	10.32	14.84	10.04	5.67	4.83	22.01	9.55	13.31	6.88	7.74	6.52	3.52	3.00	13.40	6.39	9.90	7.46	5.48
Rb	10.66	9.60	9.46	7.28	7.63	23.68	13.35	44.27	18.23	21.94	15.72	14.74	16.00	10.46	17.82	13.10	8.02	9.99
Cs	2.24	0.98	1.28	0.13	0.31	2.87	0.61	3.70	1.65	1.87	0.20	0.15	0.34	0.40	0.21	0.21	0.29	0.27
Be	0.50	0.71	0.54	0.59	0.56	0.61	0.78	0.83	0.60	0.71	0.98	0.67	0.36	0.67	0.76	0.62	0.63	0.63
Sr	727	727	505	335	711	512	532	684	574	800	374	330	600	247	236	177	231	443
Ba	323	510	203	232	241	731	576	779	336	439	1036	302	300	515	521	1171	546	336
Sc	28.89	32.22	24.52	32.40	22.66	23.05	26.20	29.36	16.11	17.81	16.33	11.90	15.00	5.25	8.39	7.46	5.99	7.39
V	523	364	285	311	220	239	228	289	162	185	132	107	120	44.28	46.95	34.44	38.15	47.69
Cr	5.54	60.66	8.97	12.86	16.75	5.95	35.90	26.01	10.16	13.71	11.00	7.66	18.00	6.56	2.95	4.94	2.98	3.01
Co	56.26	29.97	30.50	35.92	24.97	26.69	16.96	14.11	9.72	11.87	11.24	46.72	10.00	5.05	48.68	3.83	58.34	40.41
Ni	11.43	18.10	2.38	4.28	7.17	7.58	128.75	8.05	4.49	5.96	4.69	6.30	14.00	0.00	2.33	1.99	2.64	2.23
Cu	173	55.41	60.30	76.78	8.65	38.42	11.47	29.16	39.04	47.21	30.75	133.29	32.00	31.45	4.24	20.60	8.68	4.42

Table 1. (continued)
Таблица 1. (продолжение)

Sl, No.	1	2	3	4	5	6	7	8	9	10	11	12	13	14	15	16	17	18
SMP No.	Ку-4	413	427	Ку-6б	Ку-5	401	407	404-1	492	404-2	403	Ку-1	408	428	Ку-6а	412	Ку-2	Ку-3
Zn	54.63	56.34	49.79	78.12	37.29	70.00	50.94	58.23	33.23	41.33	53.94	34.17	23.00	15.56	44.11	28.63	26.33	19.26
Ga	18.10	18.72	16.30	18.29	17.04	17.10	19.10	21.60	14.56	16.75	18.95	14.94	19.00	13.90	13.30	12.53	13.49	14.18
Y	15.25	26.96	15.31	23.59	23.29	18.73	31.06	30.51	17.14	20.19	34.16	12.65	14.00	10.62	16.91	13.54	14.58	20.99
Nb	0.89	1.99	0.99	1.80	1.52	1.51	2.37	3.36	1.66	5.57	3.18	1.58	1.80	2.06	3.06	2.67	2.81	3.36
Ta	–	0.11	0.07	0.03	0.01	0.06	0.10	0.17	0.10	0.18	0.15	0.16	0.13	0.13	0.10	0.12	0.11	0.19
Zr	13.42	21.71	11.45	7.68	11.23	44.12	8.62	23.69	15.66	21.42	16.02	16.51	26.10	32.53	12.92	24.64	24.19	25.39
Hf	0.64	0.78	0.50	0.52	0.54	1.15	0.44	0.89	0.50	0.64	0.56	0.81	0.70	0.93	0.61	0.77	0.87	0.95
Pb	2.04	2.04	2.20	3.58	3.57	5.45	3.47	4.23	3.67	4.28	3.82	2.37	3.00	4.13	4.61	4.16	4.39	2.74
U	0.74	1.17	0.73	1.11	1.09	3.75	2.13	1.57	0.98	1.18	0.93	1.75	1.10	1.08	2.40	0.98	1.17	4.72
Th	1.52	1.82	1.29	1.50	1.74	5.22	2.24	4.02	2.47	2.71	1.93	4.49	4.20	2.24	5.02	2.54	4.07	7.71
La	13.71	14.67	9.20	8.57	14.11	15.69	12.55	11.53	8.34	14.32	13.90	9.26	11.00	13.44	14.75	13.02	15.21	19.70
Ce	36.44	45.95	23.55	21.93	35.79	40.80	36.55	32.59	19.81	35.59	37.57	19.93	21.00	26.18	31.30	30.61	29.80	41.51
Pr	5.26	6.11	3.51	3.15	5.19	4.63	4.52	4.00	2.57	3.83	4.43	2.45	2.40	3.05	3.81	3.20	3.51	4.83
Nd	25.16	30.06	15.96	14.57	24.62	20.22	20.01	17.69	11.46	16.13	19.98	10.14	10.00	11.60	15.05	12.96	13.41	18.57
Sm	6.23	7.45	4.14	3.94	5.79	4.24	4.48	4.16	2.64	3.45	4.80	2.23	2.00	2.40	3.12	2.59	2.75	3.85
Eu	1.87	2.01	1.21	1.11	1.52	1.07	1.18	1.14	0.80	1.04	1.01	0.80	0.60	0.76	0.82	0.74	0.66	0.94
Gd	4.99	6.47	3.45	4.08	4.96	3.36	4.03	3.98	2.50	3.08	4.61	2.17	2.30	1.64	2.80	2.23	2.48	3.36
Tb	0.63	0.85	0.47	0.66	0.71	0.52	0.68	0.67	0.42	0.51	0.77	0.35	0.30	0.26	0.45	0.35	0.39	0.56
Dy	3.38	4.94	2.94	4.35	4.39	3.37	4.70	4.69	2.95	3.49	5.36	2.23	2.00	1.94	2.89	2.41	2.50	3.73
Ho	0.60	0.92	0.58	0.93	0.90	0.68	1.00	1.00	0.62	0.74	1.12	0.49	0.40	0.39	0.63	0.49	0.53	0.81
Er	1.56	2.43	1.67	2.83	2.69	1.91	2.93	2.96	1.84	2.17	3.24	1.53	1.30	1.29	2.02	1.39	1.64	2.49
Tm	0.21	0.33	0.22	0.41	0.39	0.28	0.45	0.45	0.28	0.32	0.49	0.23	0.18	0.17	0.31	0.20	0.25	0.38
Yb	1.31	2.09	1.55	2.64	2.46	1.78	3.04	3.02	1.82	2.16	3.26	1.52	1.20	1.18	2.03	1.35	1.69	2.74
Lu	0.18	0.30	0.22	0.40	0.36	0.26	0.45	0.46	0.27	0.31	0.46	0.24	0.18	0.21	0.32	0.20	0.26	0.43
f	0.58	0.56	0.61	0.59	0.52	0.51	0.52	0.55	0.59	0.58	0.58	0.59	0.57	0.55	0.58	0.61	0.51	0.57
Sr/Y	47.6	27.0	33.0	14.2	30.5	27.4	17.1	22.4	33.5	39.6	10.9	26.1	42.9	23.2	14.0	13.1	15.8	21.1
La/Yb	10.5	7.1	5.9	3.2	5.7	8.8	4.1	3.8	4.6	6.6	4.3	6.1	7.2	11.4	7.3	9.6	9.0	7.2

Table 1. (continued)
Таблица 1. (продолжение)

Sl. No.	19**	20**	21***	22***	23*	24**	25*	26***	27*	28*	29*	30***	31*	32*	33*	34*	35**
SMP No.	С-20/ 36.0	С-29/ 4.0	КС-3/ 35	КС-3/ 17-36	С-61/ 20.0	С-30/ 6.0	С-61/ 43.0	4462	С-62/ 36	С-6Г/ 58.5	С-60/ 15.0	1506-1	С-62/ 11.0	С-63/ 35.0	С-60/ 50.5	С-3Г/ 60.0	18
SiO_2	55.82	63.22	65.20	66.36	66.36	67.50	68.28	68.60	68.68	69.34	70.06	70.44	71.40	71.74	74.56	75.22	76.00
TiO_2	0.66	0.50	0.55	0.46	0.44	0.36	0.44	0.40	0.44	0.40	0.38	0.34	0.35	0.34	0.29	0.28	0.24
Al_2O_3	18.19	17.29	15.32	15.66	14.87	15.02	14.35	15.00	15.44	15.42	14.64	14.84	14.40	14.95	13.67	13.02	13.12
Fe_2O_3	2.50	1.86	2.25	2.11	2.40	1.44	1.57	1.66	0.92	1.31	1.81	0.90	0.94	1.05	0.35	0.51	0.70
FeO	5.50	3.56	3.08	2.65	2.75	2.99	2.67	2.66	2.96	2.11	1.63	2.93	2.04	1.89	1.69	1.26	1.01
MnO	0.10	0.11	–	–	0.06	0.09	0.05	0.05	0.10	0.07	0.07	0.06	0.07	0.06	0.05	0.04	0.03
MgO	3.91	2.15	1.55	1.61	2.03	1.78	2.06	1.88	1.25	1.08	1.28	0.95	0.90	0.81	0.70	0.65	0.45
CaO	7.21	5.10	5.71	4.39	5.04	3.69	4.21	3.65	2.85	3.01	2.06	2.94	2.37	2.41	1.70	1.32	1.58
Na_2O	3.26	4.20	4.08	4.45	4.00	4.36	3.86	3.98	4.92	4.90	4.91	4.69	4.91	4.74	5.27	5.08	4.98
K_2O	0.73	1.11	0.43	0.92	0.65	1.24	0.76	1.08	1.06	1.00	1.63	1.19	1.04	0.99	0.99	0.85	0.84
P_2O_5	0.10	0.11	0.16	0.14	–	0.02	–	0.11	–	–	–	0.08	–	–	–	–	0.02
ImPs	1.10	0.64	1.16	1.35	1.43	0.58	1.50	0.77	0.89	1.17	0.80	0.80	0.88	0.96	0.88	1.05	0.27
Total	99.08	99.84	99.49	99.74	100.0	99.07	99.35	99.83	99.48	99.66	100.55	100.16	99.30	99.94	100.16	99.28	99.24
f	0.52	0.57	0.65	0.61	0.57	0.57	0.52	0.55	0.63	0.63	0.58	0.68	0.64	0.66	0.61	0.59	0.67

Note. 1–5 – blocks of gabbro, gabbrodiorite, diorite; 6–8 – dikes of microgabbro and microgabbrodiorites; 9–14 – vein trondhjemites, contaminated to varying degrees; 15–18 – trondhjemites of the main phase; 19 – metadiorite; 20–27 – tonalites; 28–35 – trondhjemites and aplites (33–35). Analyzes 19–35 – geological survey data: * – [Kubashin, Lykova, 1985], ** – [Yagovkin, Podkopaeva, 1985], *** – [Rapoport, Medyakov, 1974].
Примечание. 1–5 – габбро, габбро-диориты, диориты; 6–8 – дайки микрогаббро и микрогаббро-диоритов; 9–14 – жильные трондъемиты, в разной степени контаминированные; 15–18 – трондьемиты главной фазы; 19 – метадиорит; 20–27 – тоналиты; 28–35 – трондьемиты и аплиты (33–35). Анализы 19-35 – данные геологосъемочных работ: * – [Kubashin, Lykova, 1985], ** – [Yagovkin, Podkopaeva, 1985], *** – [Rapoport, Medyakov, 1974].

Table 2. PT parameters of mineral equilibria of rocks of the Kurmanka massif
Таблица 2. PT-параметры минеральных равновесий пород Курманского массива

SMP No.	[HB]	[HB]	[F]	[S]	SMP No.	[HB]	[HB]	[F]	[S]	SMP No.	[HB]	[HB]	[F]	[S]
Gabbro, gabbrodiorites					Microgabbrodiorites, microdiorites					Trondhjemites				
413	8.8–9.2	664–692	9.0–9.5	9.0	401	6.7–7.1	664–673	8.0–8.5	6.6–7.0	403	7.0–8.3	678–692	8.0–9.5	7.2–8.3
427	8.1–8.8	676–684	7.0–8.0	8.1–8.9	404-1	7.7	686	8.8	7.6	408	8.9–9.3	669–676	10.0	8.9–9.2
Ку-4	7.4–9.0	682–691	8.0–9.0	7.7–9.2	407	6.8–8.2	668–684	7.2–9.0	6.7–8.3					

Note. The pressures and temperatures are given in kbar and °C: HB – according to [Blundy, Holland, 1990; Holland, Blundy, 1994], F – after [Fershtater, 1990], S – according to [Schmidt, 1992].
Примечание. Значения давления и температуры приведены в кбар и °С: HB – по [Blundy, Holland, 1990; Holland, Blundy, 1994], F – по [Fershtater, 1990], S – по [Schmidt, 1992].